Chapter 2
Climate System in Northwest China

Yaning Chen, Baofu Li and Changchun Xu

Abstract A comparative analysis for detecting temperature and precipitation changes in the period 1960–2010 was conducted using data from 74 meteorological stations in China's arid northwest. Significant increasing trends ($P<0.01$) were revealed through the investigation, showing rates of 0.343 °C/10a and 6.07 mm/10a, which is higher than the global average. The winter temperature rate increased 0.486 °C/10a, while the summer temperature changed at a rate of 0.232 °C/10a. However, although precipitation increased 2.51 mm/10a in summer, it slowed in winter to a rate of 1.16 mm/10a. Regionally, the highest increasing rates of temperature and precipitation occurred in northern Xinjiang, and the lowest rates were recorded in southern Xinjiang and the Hexi Corridor. We found that, among the four seasons, winter saw the greatest temperature changes. We also found that the winter temperature in this region had a strong association with the Siberian High (correlation coefficient: $R=-0.715$) and greenhouse gas emissions ($R=0.51$).

Keywords Increased temperature change · Dynamic precipitation change · Extreme temperature and precipitation · Past climate change · Future forecast

Over the past century, carbon dioxide emissions into the atmosphere caused by human activities increased from 9.4 billion tons in 1960 to 33.5 billion tons in 2010. Accordingly, concentrations of carbon dioxide increased from 315 ppm in 1960 to 389 ppm in 2010, respectively. Meanwhile, other greenhouse gas emissions are also on the rise. Significant changes in atmospheric composition and radiative forcing

Y. Chen (✉) · B. Li
State Key Laboratory of Desert and Oasis Ecology,
Xinjiang Institute of Ecology and Geography,
Chinese Academy of Sciences, No. 818 South Beijing Road,
830011 Urumqi, Xinjiang, China
e-mail: chenyn@ms.xjb.ac.cn

B. Li
e-mail: libf@ms.xjb.ac.cn

C. Xu
Key Laboratory of Oasis Ecology, School of Resources
and Environmental Science, Xinjiang University,
No.14 Shengli Road, 830046 Urumqi, China
e-mail: xcc0110@163.com

Y. Chen (ed.), *Water Resources Research in Northwest China,*
DOI 10.1007/978-94-017-8017-9_2,

result in a severe damage to climate systems with regards to the natural energy balance, which then causes varying degrees of changes in the evolutionary processes of the natural environment (Guo 2010). The fourth assessment report of IPCC (2007) points out that the linear growth rate of the global average temperature was 0.74 °C from 1906 to 2005 and that it exceeded the rate from 1901 to 2000. On average, temperature increases were more prevalent in high latitude areas of the Northern Hemisphere, and warming was more prevalent in continents than in oceans.

Overall, climate change has exerted extensive and profound influences on the natural world. In response to these challenges, scholars have stepped up their research efforts into climate change variability, effects and forecasting. However, two disadvantages exist in climate change analysis and simulation on a global scale: the first is that simulated results are not always the same and may even vary for different simulation methods; the second is that simulated results obtained on a global scale are usually not applicable to a regional scale, which has negative impacts on the suitability of comprehensive policy-making. For these reasons alone, it is important to carry out research on regional climate change and its effects on natural and man-made environments (Tebaldi et al. 2005; Pierce et al. 2009; Mariotti et al. 2011; Ashrafi et al. 2012).

The climate of China's arid northwest region is characterized mainly by dryness. In earlier studies in this area, researchers focused on the formation and evolution of arid climacteric conditions (Zhang and Jiang 1992; Zhang et al. 2000), along with the characteristics of climate change (Chen et al. 1984; Li et al. 1995) and the projection of future climate (Shi and Zhang 1995). However, the scope and depth of research was limited. In 2002, Shi et al. (2002) pointed out that, over the past 100 years since the end of the Little Ice Age in the nineteenth century, Northwest China was in a fluctuating warm-dry period. Specifically, and using the area to the west of the Tianshan Mountains as being representative, a warm-dry to warm-wet climate emerged after 1987. Accompanying it was increasing precipitation, ice-snowmelt water and surface runoff, which resulted in increases in lake levels, flood disasters, vegetation improvements and decreasing dust storms.

Meanwhile, increasing precipitation and runoff were also found in the middle and west of the Qilian Mountains and other areas of Xinjiang. Projections by existing regional climate modes confirmed the transformation into a warm-wet climate, but the rate and magnitude of the transformation still needs further discussion. Subsequent studies confirmed the transformation (Li et al. 2003, 2011; Zhang et al. 2010a), although questions were also raised about the regional consistency of the change. Zhang et al. (2000) pointed out that Northwest China showed a warm-dry climate as a whole, except in some areas where warm-wet signals appeared. In view of the recent noticeable climate change, precipitation varied greatly, increasing in some places and decreasing in others. The evaporation potential also increased due to increasing temperatures. Overall, the arid index rose, accompanied by more frequent drought disasters. As can be seen from this brief summary, the climate change of Northwest China is complex, and viewing it from a short-term and isolated perspective cannot accurately reveal the process and development of precisely how the climate is changing.

2.1 Temperature Change

In recent years, the issues and challenges of climate change have attracted widespread social attention, and numerous scholars have researched the impacts and predictions of changing climate patterns (Abouabdillah et al. 2010; Stahlschmidt et al. 2011). Recently, regional effects have been detected to make strategies to address climate change (Moriondo et al. 2011; Segev 2010).

With recent socioeconomic development, China's northwest has become an important energy base due to its vast area and abundant resources. At the same time, its ecological system is becoming increasingly fragile and sensitive to regional climate effects. Therefore, it is important to know how changes in climate will affect the region not only from a weather aspect but also from environmental, economic, and human aspects.

To study the impact of climate change on the natural environment and human activities, it is necessary to know how the regional climate has changed in recent years. Previous scholars' research on climate changes in China's northwest reveals that the climate has generally trended warmer (Shi and Zhang 1995; Shi et al. 2007). However, analyses of temperature and precipitation changes in this region have been limited to the late 20th century or earlier (Shi et al. 2003; Xu et al. 2003; Zhang and Li 1982; Zhang et al. 2010).

In contrast, in our study, we use the latest (1960–2010) meteorological data from meteorological stations to explore historical and predicted temperature variations from different perspectives (i.e., years, seasons, decades, and so on). We also analyze relationships among temperature, precipitation, latitude, longitude, elevation and atmospheric circulations. Our intention here is to identify the direct causes of temperature change, hoping that results will provide a scientific basis for predicting future climate trends, assessing the impact of climate change, and formulating strategies to address its impact.

2.2 Characteristics of Temperature Change

2.2.1 Methods

(1) Mann–Kendall Non-Parametric Statistical Test The non-parametric Mann–Kendall method was used to detect change trends in precipitation and temperature which do not require data to comply with a certain statistical distribution. The method is used to detect possible trends in meteorological elements and is widely used in trend analysis. In the test, the null hypothesis (H0) states that the data (x_1, x_2,…, x_n) comprise a sample of n independent and identically distributed random variables. The alternative hypothesis (H1) of a two-sided test is that the distribution of x_k and x_i is not identical for all k and i. The test statistic (Kendall's S) is calculated as follows:

$$S = \sum_{i=1}^{n-1} \sum_{k=i+1}^{n} \operatorname{sgn}\left(x_k - x_i\right) \tag{2.1}$$

Time series x_i are ranked from $i = 1, 2 \ldots\ldots n-1$ and x_j from $j = i+1, \ldots, n$. Each data point x_i is used as a reference point and is compared with all other data points x_j, such that:

$$\operatorname{sgn}(\theta) = \begin{cases} 1, & \theta > 0 \\ 0, & \theta = 0 \\ -1, & \theta < 0 \end{cases} \tag{2.2}$$

If the data set is identically and independently distributed, then the mean of S is zero and the variance of S is:

$$\operatorname{var}[S] = \frac{\left[n(n-1)(2n+5) - \sum_t t(t-1)(2t+5) \right]}{18} \tag{2.3}$$

in which n is the length of the data set, and t is the extent of any given tie and denotes the summation overall ties. For larger sample sizes, statistic S is converted to Z_c (a statistic that is approximated by a normal distribution) and is calculated as follows:

$$Z_c = \begin{cases} \dfrac{S-1}{\sqrt{\operatorname{var}(S)}}, & S > 0 \\ 0, & S = 0 \\ \dfrac{S+1}{\sqrt{\operatorname{var}(S)}}, & S < 0 \end{cases} \tag{2.4}$$

The magnitude of the trend is given as

$$\beta = Median\left(\frac{x_i - x_j}{i - j} \right), \quad \forall j < i \tag{2.5}$$

in which $1 < j < i < n$. A positive value of β indicates an 'upward trend' and a negative value of β indicates a 'downward trend'.

With the null hypothesis (H0) of $\beta = 0$, where β is the slope of trend, the Mann–Kendall test rejects H0 if $|Z_c| > Z_{1-\alpha/2}$, in which $+Z_{1-\alpha/2}$ and $-Z_{1-\alpha/2}$ are the standard normal deviates and α is the significance level for the test. In this study, we use significance levels of $\alpha = 0.1$ and 0.05, with the corresponding standard normal deviates of 1.28 and 1.96, respectively.

(2) Abrupt Change Point Analysis The MK non-parametric test is widely applied to determine the occurrence of abrupt change points of meteorological and hydrologic series. Advantages of the method include simplicity of calculation, confirmation of the starting time of abrupt changes, and clear identification of the area of abrupt changes.

Let $x_1,\ldots, x_n$ be the data points. For each element x_i, the numbers r_i of elements x_j preceding it ($j<i$), such that $x_j<x_i$ are computed. Under the null hypothesis (no abrupt change point), the normally distributed statistic S_k can be calculated via the formula:

$$S_k = \sum_{i=1}^{k} r_i \quad (2 \le k \le n) \tag{2.6}$$

Mean and variance of the normally distributed statistic Sk can be given by:

$$\overline{S}_k = \frac{E(S_k) = k(k-1)}{4} \tag{2.7}$$

$$\mathrm{var}(S_k) = \frac{k(k-1)(2k+5)}{72} \tag{2.8}$$

The normalized variable statistic UF_k is estimated as:

$$UF_k = \frac{(S_k - \overline{S}_k)}{\sqrt{\mathrm{var}(S_k)}} \tag{2.9}$$

The normalized variable statistic UF_k is the forward sequence, and the backward sequence UB_k is calculated using the same equation but with a reversed series of data. When the null hypothesis is rejected (i.e., if any of the points in the forward sequence are outside the confidence interval), the detection of an increasing ($UF_k>0$) or a decreasing ($UF_k<0$) trend is indicated. The sequential version of the test used here enables detection of the approximate time of occurrence of the trend by locating the intersection of the forward and backward curves of the test statistic. If the intersection occurs within the confidence interval, it indicates an abrupt change point.

(3) Correlation Analysis Method The correlation analysis method is applied to detect the relationship between or among two or more variables. We used this method to detect correlation degrees and properties among variables. The correlation coefficient (r) is usually calculated as follows:

$$\mathrm{r} = \frac{\sum (x_i - \overline{x})(y_i - \overline{y})}{\sqrt{\sum (x_i - \overline{x})^2 \cdot \sum (y_i - \overline{y})^2}} \tag{2.10}$$

The distribution range of the correlation coefficient r is between $-1 \le r \le +1$. When the correlation coefficient is positive, the correlation between variables indicates a positive correlation; when the correlation coefficient is negative, it indicates a negative correlation. The greater the absolute value of the correlation coefficient $|r|$, the closer the degree of correlation between two variables. In addition, to determine if the correlation coefficient is meaningful or not, it is necessary to carry out a significance test.

(4) R/S Analytic Method R/S analysis is also called rescaled range analysis. It is usually applied to analyze long-term records of runoff time series (Rehman 2009; Rehman and Siddiqi 2009). Its principle is as follows. In considering the time series of annual runoff in a certain river, X(t), for any positive integer $\tau \ge 1$, the mean value series is defined as:

$$\langle X \rangle_\tau = \frac{1}{\tau} \sum_{t=1}^{\tau} X(t) \quad \tau = 1, 2, \ldots \tag{2.11}$$

The accumulative deviation is

$$X(t, \tau) = \sum_{t=1}^{t} (X(u) - \langle X \rangle_\tau) \quad 1 \le t \le \tau \tag{2.12}$$

The extreme deviation is

$$R(\tau) = \max_{1 \le t \le \tau} X(t, \tau) - \min_{1 \le t \le \tau} X(t, \tau) \quad \tau = 1, 2, \ldots \tag{2.13}$$

The standard deviation is

$$S(\tau) = \left[\frac{1}{\tau} \sum_{t=1}^{\tau} \left(X(t) - \langle X \rangle_\tau \right) \right]^{\frac{1}{2}} \quad \tau = 1, 2, \ldots \tag{2.14}$$

When analyzing the statistic rule of $R(\tau)/S(\tau)R/S$, Hurst discovered a relational expression

$$R / S \propto \left(\frac{\tau}{2} \right)^H \tag{2.15}$$

which can be used to identify the Hurst phenomenon in the time series and where H is called the Hurst exponent. Apparently, H is given by the slope coefficient of R/S versus $\tau/2$. According to (τ, R/S), H can be obtained by the least squares method (LSM) in a log-log grid.

In 1965, Hurst proved that, in an independently random series with limited variance, the exponent $H = 0.5$ and H ($0 < H < 1$) is dependent on an incidence function C(t):

$$C(t) = 2^{2H-1}\text{-}1 \tag{2.16}$$

When H>0.5, C(t)>0. This signifies that the process has a long-enduring characteristic and that the future trend of the time series will likely be consistent with the past. In other words, if the past showed an increasing trend, the future will also show an increasing trend. When H<0.5, C(t)<0, which indicates that the process has an anti-persistence characteristic and that the future trend of the time series will likely be opposite from the past. In other words, if the past showed an increasing trend, the future will assume a reducing trend. When H=0.5, C(t)=0, meaning that the process is stochastic.

(5) Kriging Method Kriging is an advanced, computationally intensive, geostatistical estimation method that generates an estimated surface from a scattered set of points with z-values. Consider a continuous field variable z(x) defined in a domain Ω. The domain is represented by a set of properly scattered nodes x_I, I=1, 2, …, N, where N is the total number of nodes in the whole domain. Given N field values, $z(x_1)$, …, $z(x_N)$, the problem is to obtain an estimate value of u at a point $x_0 \in \Omega$. Let us consider a set of nodes x_i, i=1, 2, …, n, surrounding point x_0 inside a sub-domain $\Omega x_0 \subseteq \Omega$. Here, a small letter index is used in place of a capital latter to emphasize that the numbering is referred to the sub-domain Ωx_0. The Kriging estimated value $Z^*_v(x)$ is a linear combination of $Z_v(xi)(i=1,2,...,n)$, i.e.,

$$Z^*_v(x) = \sum_{i=1}^{n} \lambda_i Z(xi) \tag{2.17}$$

where λi are the (Kriging) weights and n is the number of nodes inside Ωx_0. Kriging weights λi can be obtained by solving Kriging equations and are determined by requiring that the estimator $Z^*_v(x)$ be unbiased and optimal (minimum squared error of estimation), i.e.,

$$E\left[Z^*_v(x) - Z_v(x)\right] = 0 \tag{2.18}$$

$$Var\left[Z^*_v(x) - Z_v(x)\right] = E\left[Z^*_v(x) - Z_v(x)\right]^2 \rightarrow \min \tag{2.19}$$

Using the Lagrange method for constraint optimization problems, the requirements of minimum variance and unbiased estimator lead to the following Kriging equation system.

Ordinary Kriging is a linear geostatistical method. The Kriging approach uses the semivariogram to express spatial continuity (autocorrelation) and requires two separate steps. The first step is to calculate and model/fit the semivariogram for the whole area; the second step is a Kriging estimation of unmeasured points in the area. The semivariogram measures the strength of the statistical correlation as a function of distance. Typically, an authorized variogram model (e.g., exponential or spherical) is fitted to the experimental semivariogram values, calculated from

data, for given angular and distance classes. In bounded models (e.g., spherical and exponential), semivariogram functions increase with distance until they reach a maximum, named sill, at an approximate distance known as the range. The range is the distance at which the spatial correlation vanishes, and the sill corresponds to the maximum variability in the absence of spatial dependence.

$$E\left[Z(x)\right] = m \tag{2.20}$$

$$c(h) = E\left[Z(x)Z(x+h)\right] - m^2 \tag{2.21}$$

$$Zv(x_0) = \frac{1}{V}\int_v Z(x)dx \tag{2.22}$$

Ordinary Kriging is based on the assumption that the set of unknown values is a set of spatially dependent random variables; hence, each measurement z(xi) is a particular realization of the random variable Z(xi). In (2.23), the optimal Kriging weights λi are determined by solving the Kriging equations that result from minimizing the estimation variance while ensuring unbiased estimation of Z (x0) by Z*(x0). In Ordinary Kriging, the Kriging weight decreases as the datum location gets farther away from the location being estimated, and so negative Ordinary Kriging weights can occur. Typically, negative weights arise when the influence of a specific datum is screened by that of a closer one.

$$Z^*v = \sum_{i=1}^{n} \lambda_i Z(xi) \tag{2.23}$$

(6) Inverse Distance Weighted (IDW) Interpolation The inverse distance weighted (IDW) method was used to interpolate climate change trends. It is a simple and widely used spatial interpolation method that estimates the value at an unsampled location using the values of nearby sampled points, which are weighted inversely by their distance to the location (Ruelland et al., 2008). With a set of points, their coordinates and values are (X_i, Y_i) *and* Z_i ($i = 1, 2, \ldots, n$), the Z value at a location (X, Y) is calculated by the following equation:

$$Z = \frac{\left[\sum_{i=1}^{n-1} \frac{z_i}{d_i^2}\right]}{\left[\sum_{i=1}^{n} \frac{1}{d_i^2}\right]} \tag{2.24}$$

Where Z is the interpolated value for the location, n is the number of nearby points (a value of 12 was used in the study), and d_i is the distance from the ith nearby point to the location, which is calculated by the following equation:

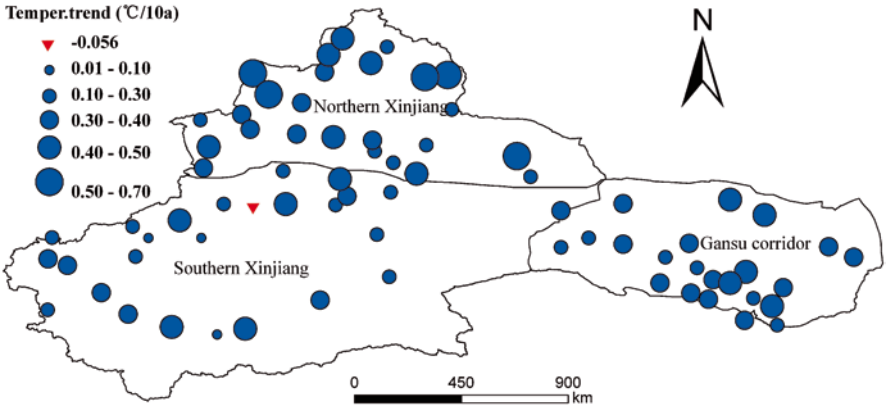

Fig. 2.1 Trends in temperature during 1960–2010

$$d_i^2 = (X - X_i)^2 + (Y - Y_i)^2 \tag{2.25}$$

2.2.1.1 Inter-Annual Variability

(1) Temperature Change in Northwest China The linear tendencies of temperature over Northwest China for the period 1960–2010 (Fig. 2.1) shows that the air temperature trended toward higher values at 73 (98.65 %) of the 74 sites analyzed in the study area. All of the positive trends are statistically significant ($P < 0.05$, under the Mann–Kendall test). The one site that does not show a significant trend has a decreasing temperature value. The increasing rate in mean annual air temperature is 0.343 °C/10a in China's northwest (Fig. 2.2), which is noticeably higher than the global rate of 0.13 °C/10a (IPCC 2007).

Regionally, temperature increases show stark differences. The temperature in northern Xinjiang increased the fastest, at a rate of 0.386 °C/10a, followed by the Hexi Corridor at a rate of 0.352 °C/10a. Southern Xinjiang showed the slowest increasing rate (0.283 °C/10a).

(2) Temperature Change in the Mountain-Oasis-Desert Areas

Trend of mean annual temperature The Mann–Kendall test found that the mean temperatures of all three landscape types showed significant increasing trends during the period 1960–2010 ($P < 0.01$), with Fig. 2.3 charting the linear tendencies of temperature at 51 stations. To some extent, this map presents the spatial distribution of temperature variation in China's arid northwest for the period under study. Of the 51 stations, only one has a slightly decreasing trend, showing a slow rate of 0.056 °C per decade; all of the others have increasing trends. The mean temperature readings of all 51 stations reveal a slight increasing trend at a rate of 0.341 °C per decade.

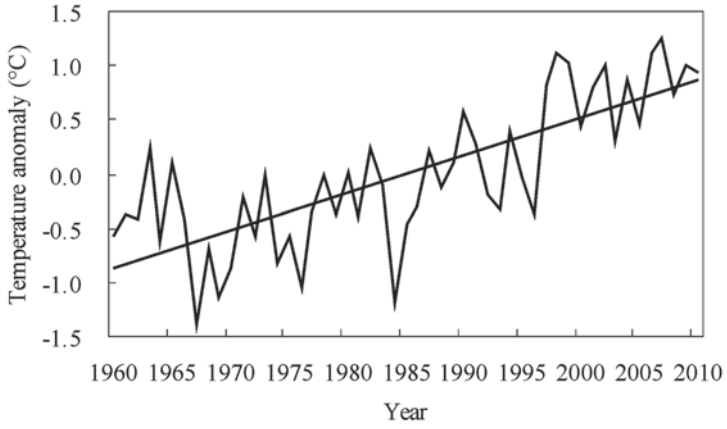

Fig. 2.2 Time series of temperature and its linear trend in ANC from 1960 to 2010

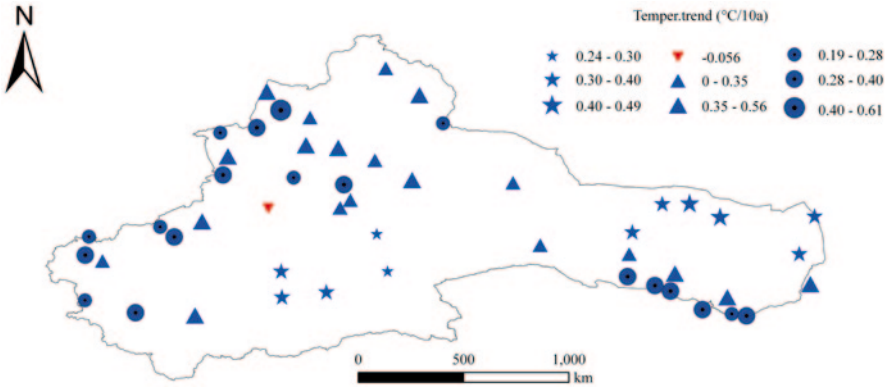

Fig. 2.3 The temperature trends at the meteorological stations in the three landscapes for the period 1960–2010

Of the three landscape types, the desert has the highest per-decade increasing rate (0.360 °C), followed by the oasis (0.339 °C) and the mountain (0.325 °C). A possible reason for the mountain having the slowest increasing rate is the widespread occurrence of snow and glaciers, along with vegetation diversity and high ecosystem stability. Mountain areas impose a certain buffer action on global climate change, while the desert region does the opposite.

To further clarify the temperature change of each area in different periods, the time series were divided into two periods: prior to the 1990s, and after the 1990s.

Prior to the 1990s, temperature trends among the 51 stations were inconsistent. For instance, seven stations (all located in the mountain and oasis areas) had decreasing trends (Fig. 2.4a). Overall, however, the trend in the 51 stations was a weak rising one, with a mean rate of 0.151 °C per decade. Sixteen of the 19 mountain

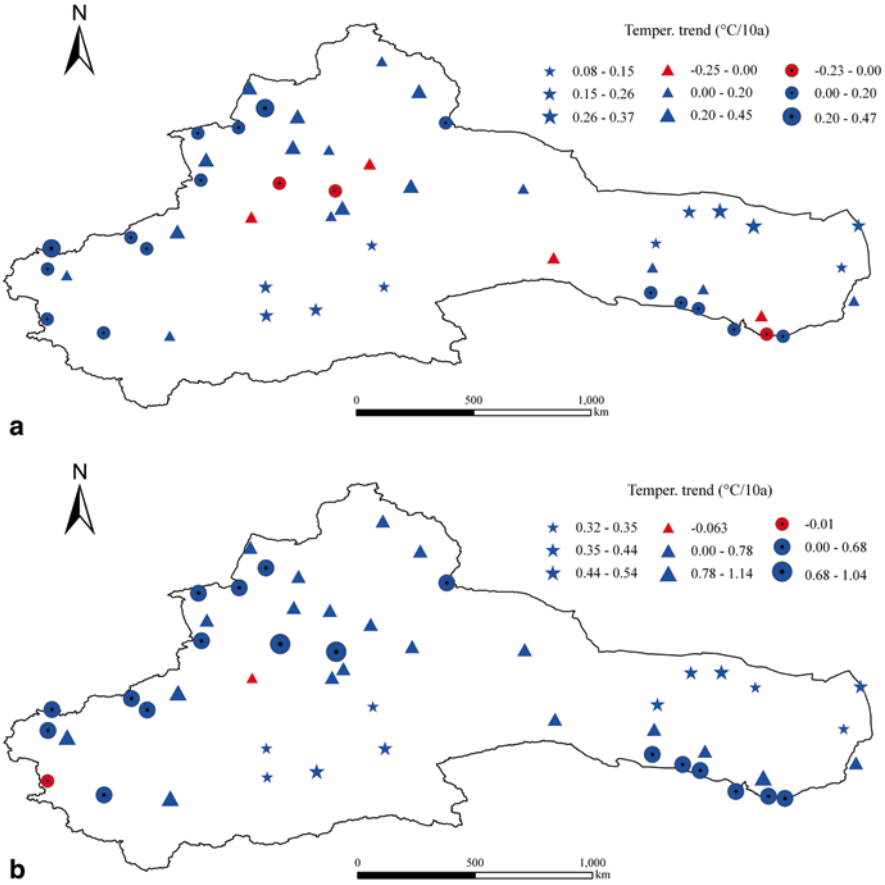

Fig. 2.4 The temperature trends in different landscapes for period **a**1960–1989 and **b** 1990–2010

stations had increasing trends, with the mean increasing rate of the mountain landscape at 0.103 °C per decade. Seventeen of the 21 oasis stations had increasing trends, with the mean increasing rate of this landscape being 0.138 °C per decade. All stations in the desert areas had increasing trends during this period, with a mean rate of 0.214 °C per decade. One reason for these variations among landscape types is that the ecosystem in the mountain area has high stability, whereas the desert ecosystem has low stability. Another reason is that the arid area of the northwest had a small population density during this time period and thus there was little human interference with the natural order of the oasis and mountain areas.

After the 1990s, the entire area experienced rapid temperature increases (Fig. 2.4b). The mean of the increasing rates at the 51 stations was 0.517 °C per decade. The oasis areas had the highest rising rate (0.60 °C per decade), followed by the mountain area (0.542 °C per decade). Both oasis and mountain areas had

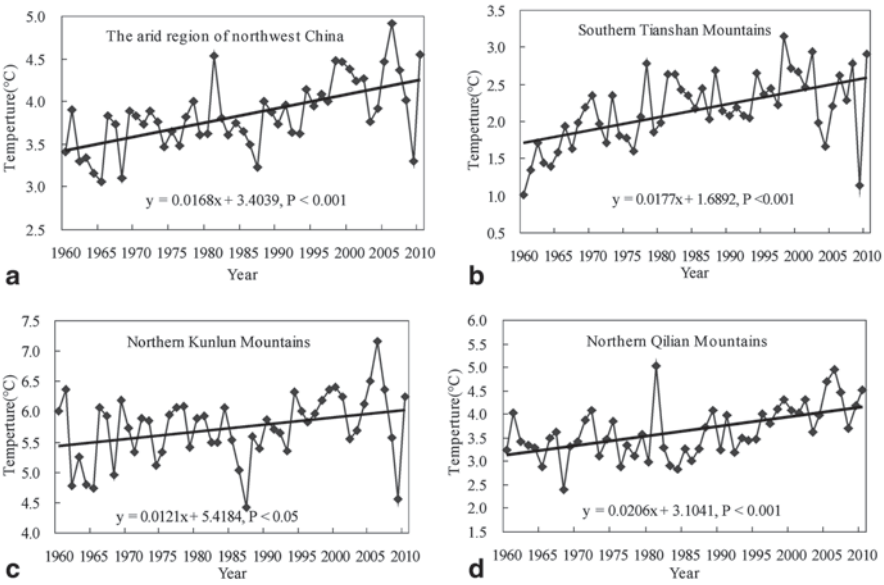

Fig. 2.5 Time series of temperature of snowmelt period and its linear trend for **a** entire northwest China, **b** southern Tianshan Mountains, **c** northern Kunlun Mountains, and **d** northern Qilian Mountains from 1960 to 2010

95% of their stations showing increasing trends, and while all stations in the desert areas had increasing trends, their mean rate was only 0.402 °C per decade, the lowest among the three landscapes. We suspect that human activity was a major factor contributing to the formation of this pattern. Since 1990, China's arid northwest has experienced rapid population growth along with rapid expansion of industrialization, tourism, and urbanization. Greenhouse emission and the "urban heat island" effect may contribute to variations among different landscapes over the background of global warming and regional climate change.

Trend of Snowmelt Period Temperature in the Mountain Area During the 1960–2010 timeframe, the mean air temperature of the snowmelt period in the northwest mountainous areas of China exhibited an upward trend, with an increasing rate of 0.168 °C/10a. This increasing trend carries a $P < 0.001$ level of significance (Fig. 2.5a). Over the past 51 years, the air temperature in the snowmelt period increased by 0.857 °C, which is higher than the world average (Brohan et al. 2006; IPCC 2007) for the same period.

Figs. 2.5b, c and d show the temporal variations of linear tendencies of the temperature of snowmelt periods over different areas from 1960 to 2010. From this figure, it can be seen that all parts of the northwest mountainous areas of China have a positive temperature tendency during their snowmelt periods. The northern Qilian Mountains have a relatively high positive tendency, whereas low positive tendencies are observed in the southern Tianshans and northern Kunlun Mountains.

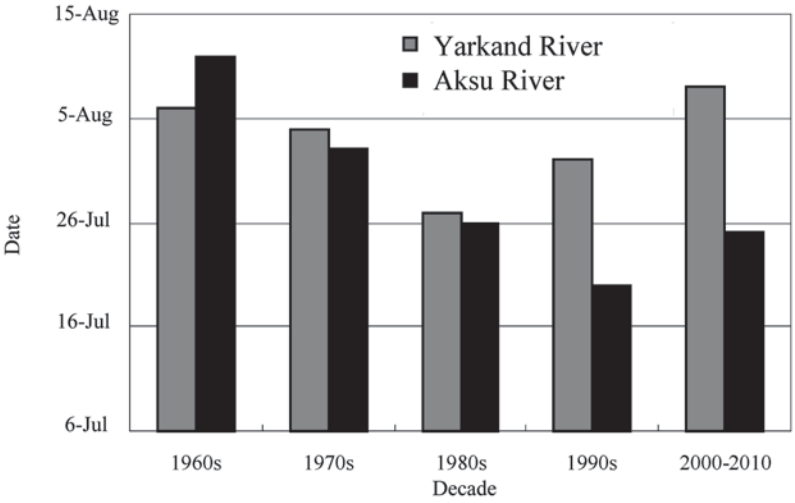

Fig. 2.6 The date of maxima daily temperature (9 day moving mean) in every decade over Aksu River and Yarkand River

However, all of these trends are statistically significant ($P<0.05$, under the Mann–Kendall test).

Regionally, temperatures during the snowmelt period in the northern Qilian Mountains increased the fastest (1.05 °C), followed by those in the southern Tianshan Mountains (0.903 °C). However, temperatures in the northern Kunlun Mountains increased the slowest, by only 0.617 °C.

Next, we take the Aksu and Yarkand Rivers as objects for further analysis on the date change of the maximum daily mean temperature in different decades (a 9-day moving average). For the period 1960–2000, the date of the maximum daily temperature in the Aksu River moved ahead 22 days (Fig. 2.6) compared with that in 1990s, while the date was delayed 5 days for the period 2000–2010 (which is basically consistent with that in the 1980s). The maximum daily temperature in the Yarkand River occurred 10 days ahead in 1960s–1980s, while the date was delayed in 1990–2010. However, the date for the period 2000–2010 was basically consistent with that in the 1960s.

Overall, the dates for maximum daily temperature in the mountains appear earlier in the 1970s and 1980s, while the date has been delayed in the first decade of the twenty-first century.

(3) Temperature Changes in Typical Rivers In this section, 11 rivers of five typical river areas in three typical areas in China's arid northwest zone form the research topic (Table 2.1). The three typical areas are northern Xinjiang (the south slope of the Altai Mountains and the north slope of the Tianshan Mountains), southern Xinjiang (the north slope of the Kunlun Mountains and the south slope of the Tianshan Mountains) and the Hexi Corridor (the north slope of the Qilian Mountains), which basically includes all of the main inland rivers in China's arid region

Table 2.1 The rivers and weather stations information in the arid region of Northwest China

Areas	Typical river areas	Rivers	Weather stations (Information sessions)
Hexi Corridor	The north slope of Qilian Mountains	Heihe	Qilian (1957–2010)
		Shiyang River	Wushaoling (1957–2010)
		Shule River	Tuole (1957–2010)
Northern Xinjiang	The south slope of Altai Mountains	Kelan River	Altai (1957–2005)
	The north slope of Tian-shan Mountains	Urumqi River	Daxigou, Yingxiongqiao (1957–2006)
		Manas River	Kenswatt (1957–2006)
		Kuitun River	Jialeguola (1957–2006)
Southern Xinjiang	The south slope of Tian-shan Mountains	Aksu River	Toergate, Aheqi (1957–2010)
		Kaidu River	Bayinbuluke (1957–2010)
	The north slope of Kunlun Mountains	Hotan River	Hotan (1957–2010)
		Yarkand River	Taxkorgan (1957–2010)

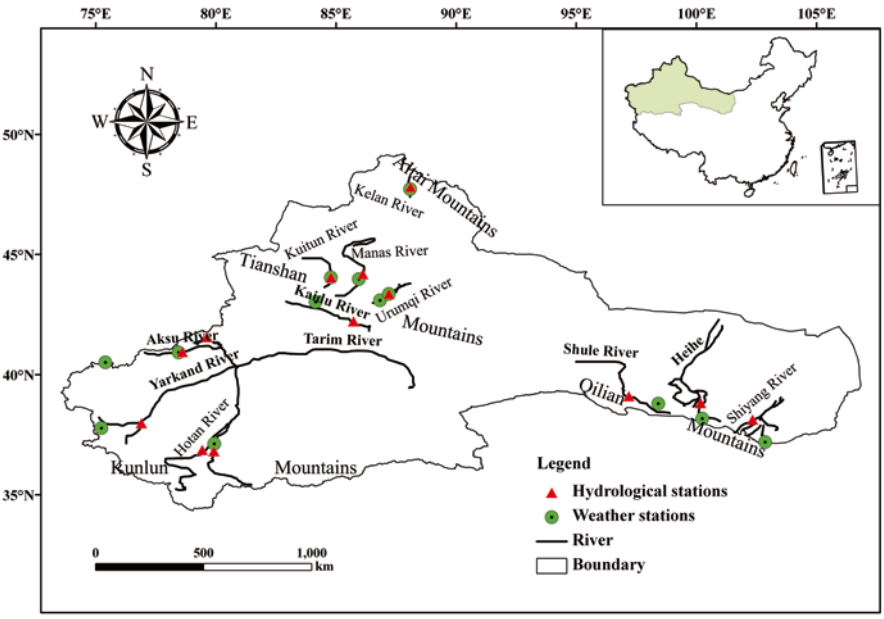

Fig. 2.7 The weather and hydrological stations of rivers in the arid region of northwest China

(Fig. 2.7) (Li et al. 2012a). To minimize the impact of human activities and make the regional climate changes more clear, data from the selected weather stations represent climate changes for each mountain area. We use the mean value of the data to represent temperature and precipitation.

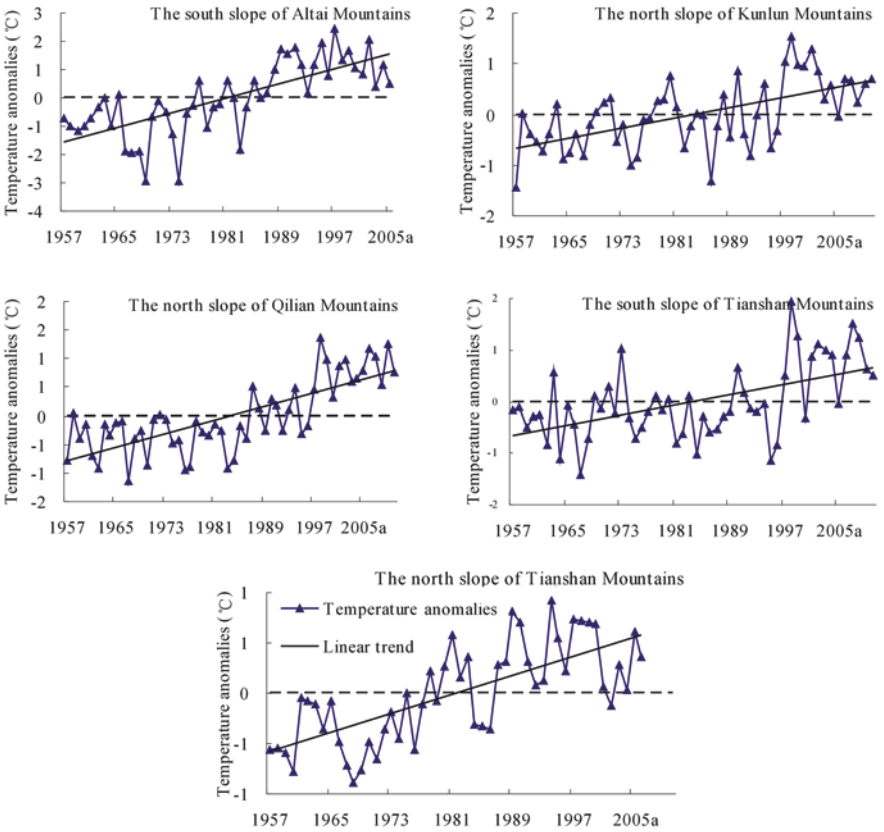

Fig. 2.8 Temperature anomalies trends in typical river areas in the arid region of Northwest China

Over the past five decades, the temperature in each river area (the south slope of the Altai Mountains, the north slope of the Kunlun Mountains, the north slope of the Qilian Mountains, and the south and north slopes of the Tianshan Mountains) has increased, fluctuating at an average rate of 0.32 °C per decade (Fig. 2.8) (Li et al. 2012). The temperature on the south slope of the Altai Mountains rose the fastest, increasing by 0.64 °C/10a; the second fastest increase (0.29 °C/10a) occurred on the north slope of the Qilian Mountains, while the slowest increases occurred on the south (0.24 °C/10a) and north (0.24 °C/10a) slopes of the Tianshan Mountains and on the north slope (0.25 °C/10a) of the Kunlun Mountains. In addition, the Mann–Kendall test showed that the increasing temperature trend in each river area was statistically significant, at $P < 0.01$ (Table 2.2).

From the perspective of coefficients of variation, temperature variations were the largest on the north slope of the Qilian Mountains, indicating strong variability. This was followed by temperature variations on the southern slopes of the Altai and Tianshan Mountains, suggesting moderate variability, while temperature variations

Table 2.2 Temperature trends and tests in different typical river areas in the arid region of northwest China

Areas	Typical river areas	Cv	Zc	Step change points	Periods (a)
Hexi Corridor	The north slope of Qilian Mountains	1.252	4.68**	1994**	19**
Northern Xinjiang	The south slope of Altai Mountains	0.327	5.53**	1984**	19**
	The north slope of Tianshan Mountains	0.087	5.14**	1978**	17**
Southern Xinjiang	The south slope of Tianshan Mountains	0.148	2.65**	None	20*
	The north slope of Kunlun Mountains	0.083	3.76**	(1980,1987)**	19**

*$P<0.05$; **$P<0.01$

on the north slopes of the Tianshan and Kunlun Mountains were the smallest, pointing to weak variability (Table 2.2).

2.2.1.2 Seasonal Variability

From 1960 to 2010, spring air temperatures trended to larger values at 73 (98.65%) of the 74 sites (Fig. 2.9), declining at only 1 site. Most of the upward trends were statistically significant ($P<0.05$, under the Mann–Kendall test). At sites registering no significant trends, temperature values increased at 8 stations (10.96% of all sites), and declined only at 1. The increasing rate of mean air temperature was 0.268 °C/10a across the entire arid region. Specifically, the increasing rate of temperature in northern Xinjiang was the highest (0.286 °C/10a), followed by the rates in the Hexi Corridor (0.270 °C/10a) and southern Xinjiang (0.248 °C/10a) (Table 2.3).

In summer during the period under study, the air temperature generally increased at 67 (90.54%) sites and decreased at the remaining 7, and the majority of the positive trends were significant ($P<0.05$, under the Mann–Kendall test). Of the stations showing no significant trends, 6 sites (8.96%) showed rising temperature trends and 3 showed declining temperature trends. The rising rate of mean summer air temperature was 0.232 °C/10a in the study area, which is lower than that in spring. The rising rate of temperature was the highest in the Hexi Corridor (0.292 °C/10a), followed by northern Xinjiang (0.231 °C/10a) and southern Xinjiang (0.173 °C/10a) (Table 2.3).

In autumn for the same time period (1960–2010), the air temperature increased at 72 sites (97.30% of total) and decreased at the other 2 sites. The trends were significant ($P<0.05$) at all sites except for the 2 (2.78% of total). The rising rate of mean temperature was 0.360 °C/10a, which is notably higher than the rates in spring and summer. Northern Xinjiang had the highest rate of temperature increase

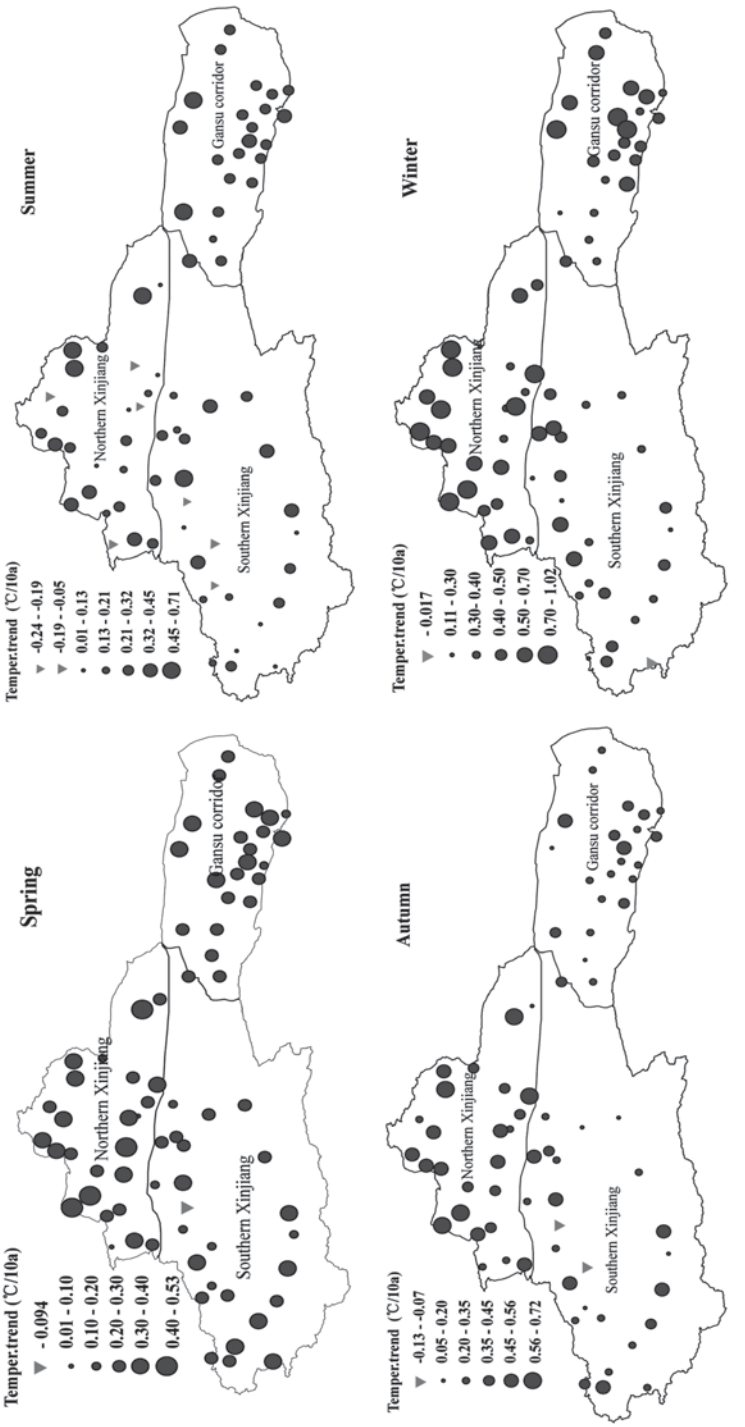

Fig. 2.9 Seasonal temperature trends in the arid region of Northwest China

Table 2.3 The annual and seasonal trend in temperature over different regions

Region	Spring (°C/10a)	Summer (°C/10a)	Autumn (°C/10a)	Winter (°C/10a)	Annual (°C/10a)
ANC	0.268**	0.232**	0.360**	0.486**	0.343**
Northern Xinjiang	0.286*	0.231**	0.451**	0.587**	0.386**
Southern Xinjiang	0.248*	0.173**	0.303**	0.385**	0.283**
Hexi Corridor	0.270**	0.292**	0.326**	0.486**	0.352**

*$P<0.05$; **$P<0.01$

(0.451 °C/10a), followed by the Hexi Corridor (0.326 °C/10a) and southern Xinjiang (0.303 °C/10a).

In winter over the same 50-year time frame, the air temperature trended toward higher values at 73 (98.65%) of the 74 stations (Fig. 2.9) and toward a lower value at the 1 remaining site. The trends were all statistically significant ($P<0.05$) except at 5 sites (6.85% of total) that showed rising temperatures and 1 site that showed declining temperature. The increasing rate of mean air temperature was 0.486 °C/10a, which is higher than that in spring, summer and autumn. The increasing rate of temperature in northern Xinjiang was the highest (0.587 °C/10a), followed by the Hexi Corridor (0.486 °C/10a) and southern Xinjiang (0.385 °C/10a) (Table 2.3).

2.2.1.3 Decadal Variability

In the 1960s, the mean temperature in China's arid northwest was 6.453 °C; by the 1970s, it had increased only by 0.045 °C. Overall, however, the temperature had risen at 55.41% of the meteorological stations. The sites with temperature reductions were located mainly in the southern Tianshan Mountains and in eastern Xinjiang. Temperature increases occurred in southern Xinjiang (0.11 °C), followed by the Hexi Corridor (0.029 °C) and northern Xinjiang (0.016 °C) (Fig. 2.10).

In the 1980s, the mean temperature in the study area rose by 0.297 °C, which was a more substantial increase than during the 1970s. Overall, the temperature at 83.78% of the meteorological stations had increased. The sites with temperature declines were located mainly in the Qilian Mountains. Temperature increased the most in northern Xinjiang (0.466 °C), followed by the Hexi Corridor (0.249 °C) and southern Xinjiang (0.153 °C).

In the 1990s, the mean temperature increased by 0.507 °C, which was a faster rate of increase than the 1960s, 1970s, or the 1980s. Overall, the temperature increased at 87.84% of the meteorological stations. Temperatures in the Hexi Corridor and in northern Xinjiang increased by 0.597 °C and 0.564 °C, respectively, while the temperature in southern Xinjiang increased only slightly (0.356 °C).

During the period 2000–2010, the mean temperature showed a continuous increasing trend. However, the increasing rate was 0.487 °C, which is less than in the 1990s, and 9.5% of the stations showed declining temperatures. Moreover, there

Fig. 2.10 Temperature trends by decade in the arid region of northwest China

Table 2.4 Results of Mann–Kendall test for annual and seasonal precipitation and temperature

Parameter	Annual	Spring	Summer	Autumn	Winter
Precipitation (mm/decade)	8.01[b] (172.38)	1.78 (43.93)	2.55[a] (78.48)	1.72[a] (35.50)	1.73[b] (13.80)
Temperature (°C/decade)	0.35[b] (7.20)	0.24[a] (9.18)	0.26[b] (17.75)	0.41[b] (7.40)	0.39[b] (–8.83)

The data in the parenthesis are the mean of the study area
[a, b] delineate the significance at 5%
[b] delineate the significance at 1% significance level

were only slight differences in the extent of temperature increases in the Hexi Corridor, northern Xinjiang, and southern Xinjiang, with increases of 0.483 °C, 0.415 °C, and 0.571 °C, respectively.

2.2.1.4 Spatio-Temporal Distribution of Monotonic Trends

In Table 2.4, the regional MK trends for annual and seasonal air temperatures are investigated. For air temperature, significantly increasing trends occurred across the entire region for all seasons. The most significant change occurred in autumn, with a regional trend magnitude of 0.41 °C/decade.

The spatial distribution pattern of temporal trends for air temperature at both individual stations and at basins (Fig. 2.11 and Fig. 2.12) shows that, for annual air temperature, about 97% of the stations had a significant trend ($P<0.05$), and that all of the basins showed statistically significant increases ($P<0.01$), especially the Cherchen River, the Bayi Basin and the Heihe River (Fig. 2.12a). About 61% and 73% of the stations had statistically significant increasing trends in spring and winter, respectively (Figs. 2.11b, e). Moreover, the spatial distribution of trends in spring also had the same pattern as those in winter, with stations in southern Xinjiang and the Hexi Corridor showing larger trend magnitudes (Figs. 2.12b, e). Regarding summer-time air temperature, 80% of the stations exhibited statistically significant trends (Fig. 2.11c), and all of the basins (except for the rivers in the eastern section of the north slope of the Tianshan Mountains [the NSET Rivers], the Weigan River and the Yarkand River) showed significant changes at a 0.05 significance level (Fig. 2.12c). Similarly, in autumn, approximately 95% of the stations demonstrated statistically increasing trends (Fig. 2.12d), with the Hotan and Aksu River basins exhibiting the most significant changes compared to other basins (Fig. 2.12d). It can therefore be concluded that the air temperature increased significantly, resulting in a warmer climate in the arid region of northwestern China.

2.2.1.5 Spatial Distribution Characteristics of Temperature Extremes

Minimum temperature The spatial distribution of minimum temperature in the arid region of northwest China is inconsistent, ranging from 2.4 to 4.7℃

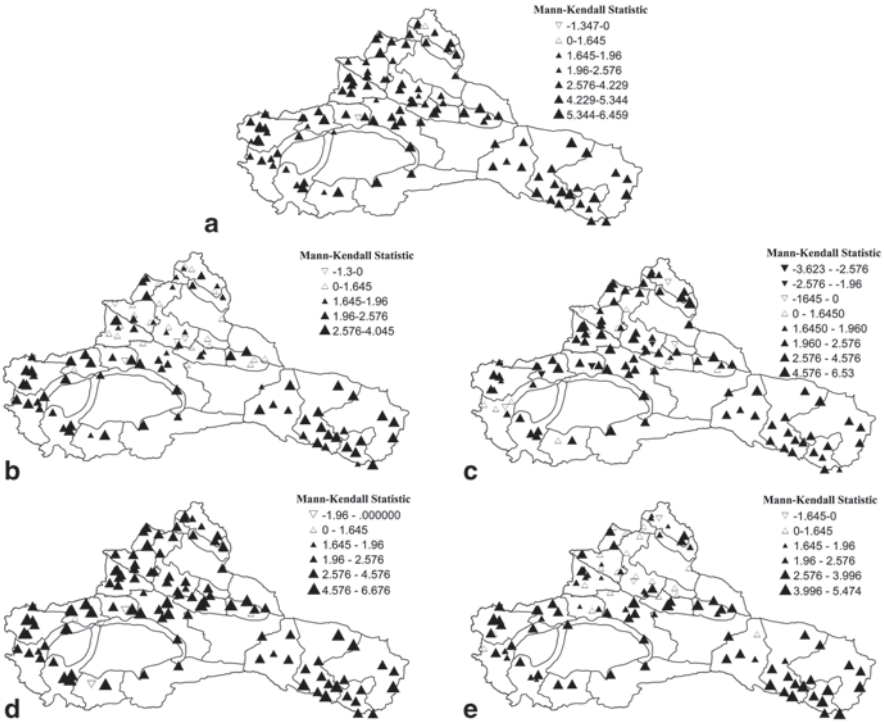

Fig. 2.11 Distribution of Mann–Kendall trends of air temperature: **a** annual, **b** spring, **c** summer, **d** autumn, **e** winter

(Fig. 2.13a). The highest minimum temperature region is located in the eastern portion of the northern slope of the Kunlun Mountains, at a range of 3–4.7 °C. In the outer ring of this area, the minimum temperature reduces to 2–3 °C. In the vast area of the Tianshan Mountains and part of eastern Xinjiang, the minimum temperature ranges from 0 to 2 °C. The minimum temperature in the northern Tianshan Mountains, including the central Hexi Corridor, is the lowest in the study area, with an average annual minimum temperature reaching −2.4 °C. Thus, we can see that the minimum temperature distribution is quite similar to the mean temperature distribution, which, to a certain extent, suggests that the minimum temperature has a larger influence on the average annual temperature.

The trend magnitude (Z value) for minimum temperature (Fig. 2.13b) shows a clear rising trend. Even the lowest Z value can reach up to 4.0 ($P < 0.01$). In most of the region under study, Z values range from 5 to 6, except in three sites, where the Z value is greater than 6. In southern Xinjiang and the northern Qilian Mountains, the Z value reaches 4.5. The uneven distribution of the Z value indicates that the minimum temperature has increased sharply, far more than the variation of mean temperature, though the scopes of minimum temperature are different.

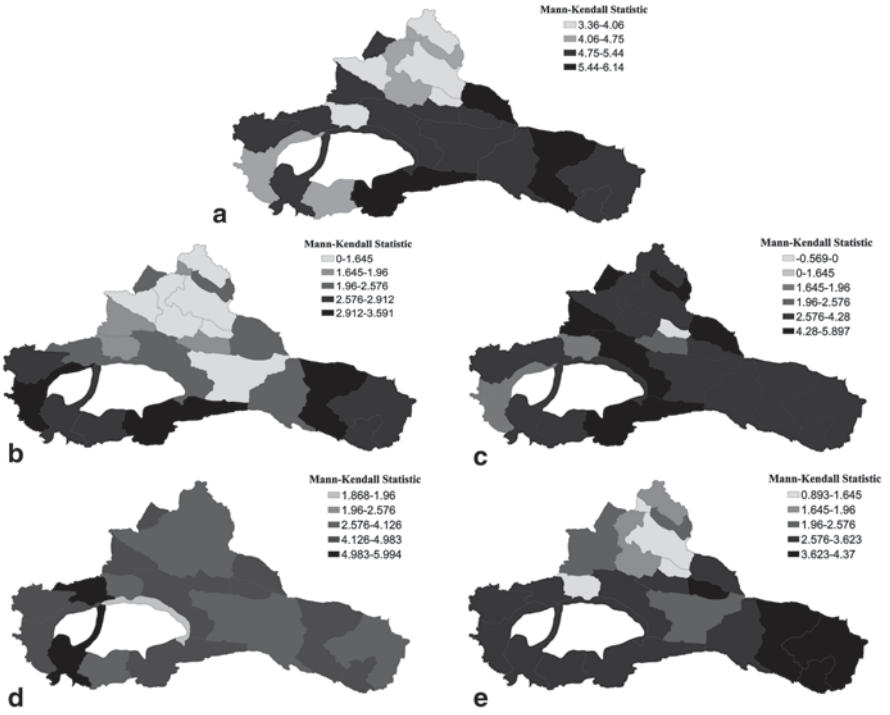

Fig. 2.12 Regional trends of air temperature at basin scale: **a** annual, **b** spring, **c** summer, **d** autumn, **e** winter

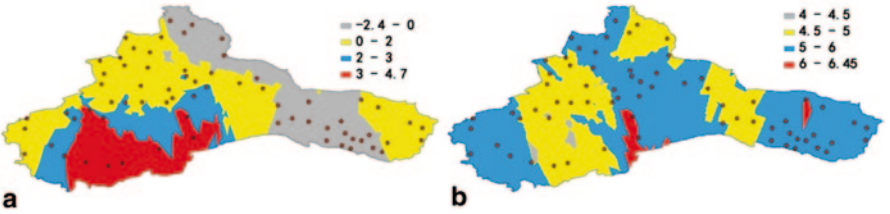

Fig. 2.13 **a** Minimum temperature distribution and **b** trend variation Z in the arid region of Northwest China

Maximum Temperature The distribution change for maximum temperature is similar to that of average and minimum temperature (Fig. 2.14a), showing a latitude-orientation characteristic. In other words, the higher the latitude, the lower the maximum temperature. Maximum temperature ranges from 10 to 19 °C, with great spatial variation. In the northern slope of the Kunlun Mountains, maximum temperature ranges from 17 to 19 °C. In the Altai, Alashan and the northern slope of the Qilian Mountains, maximum temperature ranges from 11 to 14 °C. In the rest of study area, it ranges from 14 to17 °C.

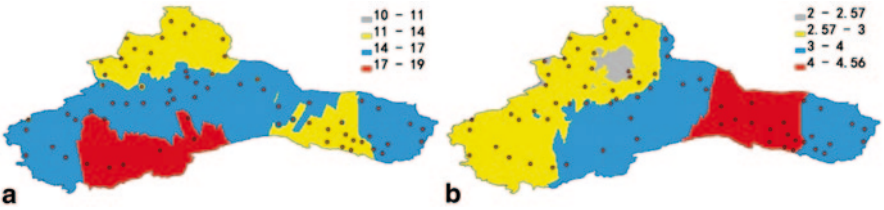

Fig. 2.14 **a** Maximum temperature distribution and **b** trend variation Z in the arid region of Northwest China

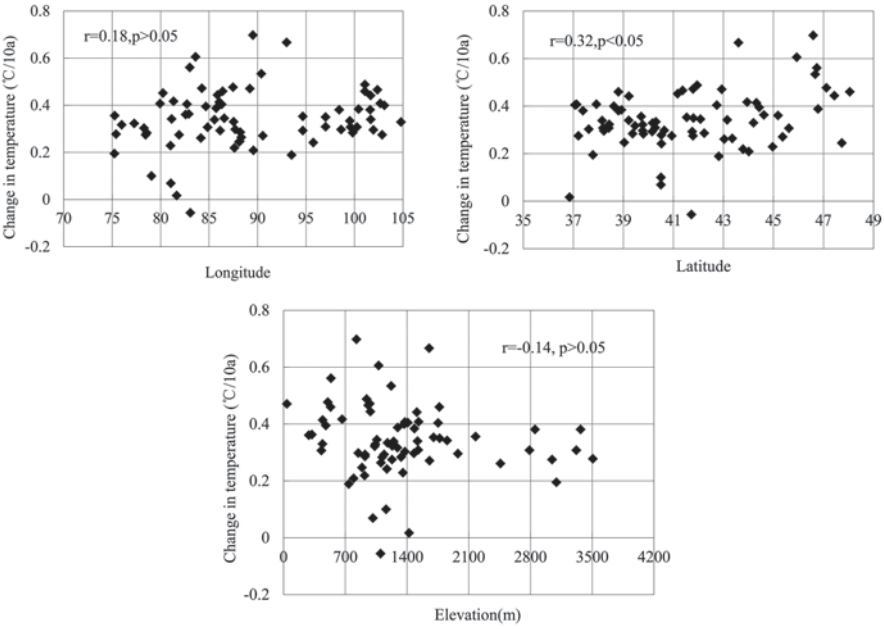

Fig. 2.15 Relationship between the trends in temperature and elevation, latitude and longitude

The Z value distribution for maximum temperature shows that it increases gradually from west to east, and then reduces slightly beyond the central Hexi Corridor, with a Z value from 3 to 4 (Fig. 2.14b). Except for a small area on the northern slope of the Tianshan Mountains, the Z values for the rest of the area meet the significance level of 0.01. Overall, the Hexi Corridor sees the greatest maximum temperature increases.

The influences of elevation, longitude and latitude on seasonal temperature trends are examined by correlation analysis (Fig. 2.15, Table 2.5). The results show that there is no significant association between the spring temperature trend and any other factor. However, the correlations between summer temperature trends and longitude are significant (at the $P<0.05$ level of significance) and the impact

Table 2.5 The relationship between seasonal temperature trends and longitude, latitude and elevation

Item	Spring (°C/10a)	Summer (°C/10a)	Autumn (°C/10a)	Winter (°C/10a)	Annual (°C/10a)
longitude	0.02	0.31*	0.05	0.16	0.18
latitude	0.14	0.06	0.38*	0.42**	0.32*
elevation	0.18	0.13	0.06	0.36*	−0.14

*$P<0.05$; **$P<0.01$

of latitude on autumnal temperature trends is also significant ($P<0.05$), as are the effects of latitude and elevation on winter temperature trends ($P<0.05$).

Although our results show only a weak correlation between trends in temperature and elevation and temperature and latitude/longitude, some researchers find that climate changes are related to elevation (Beniston and Rebetez 1996). Nonetheless, our results are consistent with other recent studies (Vuille and Bradley 2003). Although the relationship is not simple or linear, reductions in latitude generally coincide with decreases in the rate of temperature change, and some increases in latitude coincide with increases in the rate of temperature change (Fig. 2.15), which is consistent with previous research (He et al. 2005; Lu 2009).

2.2.2 Step Change Detection for Temperature

The Mann–Kendall method was used to detect step changes in temperature in the arid region of Northwest China. Results show that step changes probably occurred in 1988 ($P<0.01$) for regional annual air temperature (Fig. 2.16), but no similar results can be found at a seasonal scale. Step changes in 1998, 1996, 1987 and 1986 ($P<0.05$) were detected for spring, summer, autumn and winter for the whole region, respectively. Regarding basin scales, step changes in annual air temperature occurred in 1988 for 17 basins and in 1996 for 10 basins. Step changes at a seasonal scale were found in 1998 for spring (15 basins), in 1996 for summer (21 basins), in 1986 for autumn (15 basins), and in 1985 for winter (19 basins). This shows that the step-change point years on a basin scale are in accordance with the results for the entire arid region. Thus, for example, step changes for annual air temperature were observed in 1988.

Step change detection was done for temperature in the mountain, oasis and desert areas (Fig. 2.17). It was found that step changes occurred first in the desert area in 1987, followed by changes in the oasis area in 1990 and in the mountain area in 1997 ($P<0.05$). For the five typical river areas, step changes ($P<0.01$) were found in the northern slope of the Qilian Mountains in 1994, the southern slope of the Altai Mountains in 1984, the northern slope of the Tianshan Mountains in 1978, and in the northern slope of the Kunlun Mountains in 1980 and 1987. However, the southern slope of the Tianshan Mountains, a step change was not found (Table 2.2).

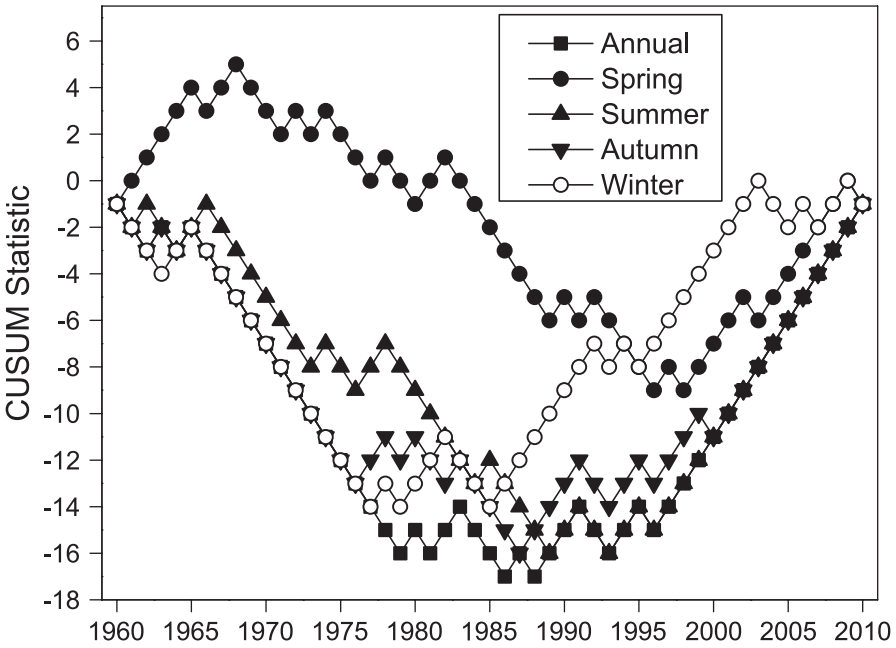

Fig. 2.16 Cumulative sum (CUSUM) charts for annual and seasonal air temperature

2.2.3 Potential Causes of Winter Temperature Change

2.2.3.1 Increasing Temperature

The Mann–Kendall (MK) statistical test revealed a significant rising trend in air temperature in the arid region of Northwest China from 1960 to 2010 ($P<0.001$), at a rate of 0.343 °C/decade. These values are consistent with results from previous research (Shi and Zhang 1995; Wang et al. 2008; Zhang et al. 2010). A rising trend was found in both oasis areas and mountainous areas, with a lower changing rate in the mountainous areas (0.325 °C/decade) and a higher rate in the oasis areas (0.35 °C/decade). Even the lower rate in the mountainous areas, however, is much higher than the average for China (0.25 °C/decade) (Ren et al. 2005) or the average of the entire globe (0.13 °C/decade) (Brohan et al. 2006; IPCC 2007). Due to the relatively low population density in China's arid region, we do not consider human activities as a major factor driving the overall regional temperature change to deviate considerably from the national and global trends. The finding that the temperature of China's northwest is quickly on the rise is consistent with results from previous research (Wang et al. 2008; Zhang et al. 2010; Sun et al. 2010) and with the statement in the Fourth Assessment Report of Intergovernmental Panel on Climate Change (IPCC) that the mid-high latitude regions of the northern hemisphere are experiencing a high rate of temperature increase.

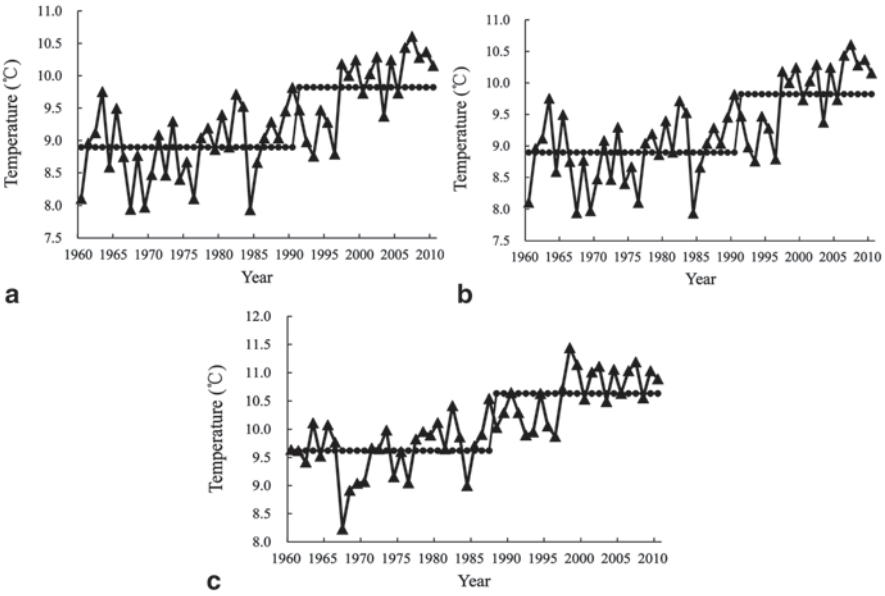

Fig. 2.17 Temperature step changes in **a** mountains, **b** oasis, **c** desert landscapes

The importance of the change of one season in an annual change is quantified as its proportion in the total change of the four seasons. This proportion was calculated for the four seasons of each year from 1981 to 2010, a process that can be represented as follows:

$$I_{s,i} = \frac{|T_{s,i} - \overline{T}_{s,1960-1980}|}{\sum |T_{s,i} - \overline{T}_{s,1960-1980}|} \times 100 \tag{2.26}$$

$$s \in \{spring, summer, autumn, winter\}$$

where $I_{\text{winter},\,i}$ is the importance of the winter temperature variation of year i in the overall temperature variation of the same year, and in this study i=1981, 1982, …2010; $T_{\text{winter},\,i}$ is the winter temperature of year i; $\overline{T}_{\text{winter},1960-1980}$ is the average winter temperature from 1960 to 1980; and $T_{s,\,i}$ is the seasonal temperature of year i.

Using Eq. (2.26), we calculated the seasonal importance in the yearly change for each year between 1981 and 2010. Over this period, the mean importance values for spring, summer, autumn, and winter were 19.3%, 13.7%, 23.6%, and 43.4%, respectively (Fig. 2.18). For the period 1984–1995, during which SHI was the weakest in the past 50 years, the importance of winter change was 57.01%. These results suggest that winter temperature change is the most important factor affecting the rising annual air temperature in China's arid northwest.

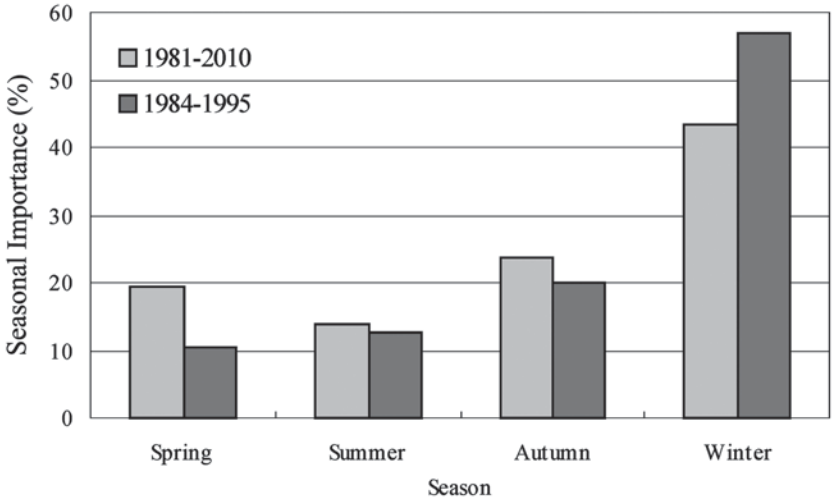

Fig. 2.18 The seasonal importance of temperature changes in different periods (1981–2010, 1984–1995)

Table 2.6 The correlation coefficients between the winter temperature in the entire region (the Arid Region of Northwest China), mountains, oases and certain factors that may affect the temperature

Factor	SOI	AAOI	NAOI	AOI	PNAI	WCI	SHI	CDE
Entire region	−0.256	0.128	0.329*	0.371*	0.023	0.377*	−0.715**	0.510**
Mountains	−0.238	0.078	0.220*	0.276	0.021	0.236	−0.629**	0.498**
Oases	−0.255	0.177	0.350*	0.388*	0.033	0.402*	−0.723**	0.504**

*$P<0.05$; **$P<0.01$

2.2.3.2 Potential Causes of Winter Temperature Change

The Pearson's correlation coefficient values (Table 2.6) show that the winter temperatures in Northwest China have a strong and significant correlation with the Siberian High Index (SHI, $R=-0.715$, $P<0.001$) and with China's carbon dioxide emissions (CDE, $R=0.51$, $P<0.001$). For all of the other tested atmospheric circulations, the correlations are much weaker and less significant. Another feature worth mentioning is that the correlations in oases are higher than in those in mountains, which means that the impact of atmospheric circulation on temperatures in oases are stronger than in mountains. In general, the Siberian High and the winter temperatures in the region have an almost perfect "mirroring" relationship during the 1960–2010 period, suggesting a direct impact of the former on the latter (Fig. 2.19). Particularly, the Siberian High intensity in the region had a deep "valley" between the late 1980s and the mid-1990s, which confirms the findings of D'Arrigo et al. (2005), Panagiotopoulos et al. (2005), and Gong and Ho (2002), who contend that the 1980s and 1990s was the weakest period for the Siberian High in the past 100 years. The aforementioned 'valley' of the Siberian High intensity coincides with

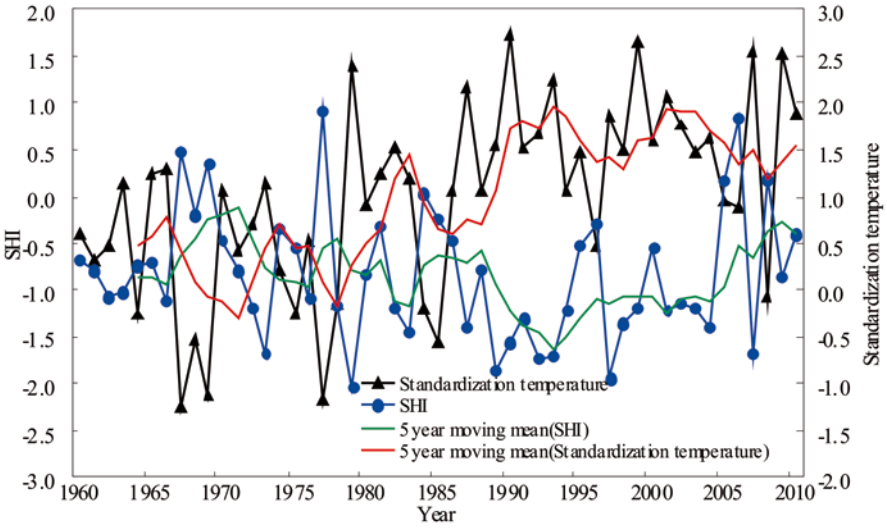

Fig. 2.19 The Siberian High Intensity and the winter temperature in the arid region of northwest China

the most obvious peak in winter temperatures in the region. Recently (2005–2010), however, the winter air temperature has been falling, along with the Siberian High intensity's recovery.

Excessive greenhouse gas emissions are generally regarded as the main cause of global warming (Crowley 2000; Mahlstein and Knutti 2010; IPCC 2007). However, as shown by Fig. 2.20, while the carbon dioxide emissions in the past 20 years maintained a strongly increasing trend, the winter temperature did not follow suit. It can be inferred from this that the rising winter temperature during the 1960–2005 period seems to be more associated with the Siberian High than with China's carbon dioxide emissions.

The R value calculated by Gong and Ho (2002) for the Siberian High intensity and air temperature in mid-to-high latitude Asia (30N–70N, 30E–40E) was −0.58, lower than that of China's arid region (−0.715). This suggests that the Siberian High had a stronger influence on air temperature in China's northwest than in other regions.

2.2.3.3 Contribution of the Siberian High to Increasing Winter Temperatures

The relationship between the change rate of the Siberian high in the 1961–2010 period and the winter temperature change rate of the same period was investigated (Fig. 2.21a). Not only did the fitting equation pass the 0.01significance level test, but in addition, the slope of the fitting equation (0.0466) was the elasticity coefficient of winter temperature change to the Siberian high change, meaning that if the

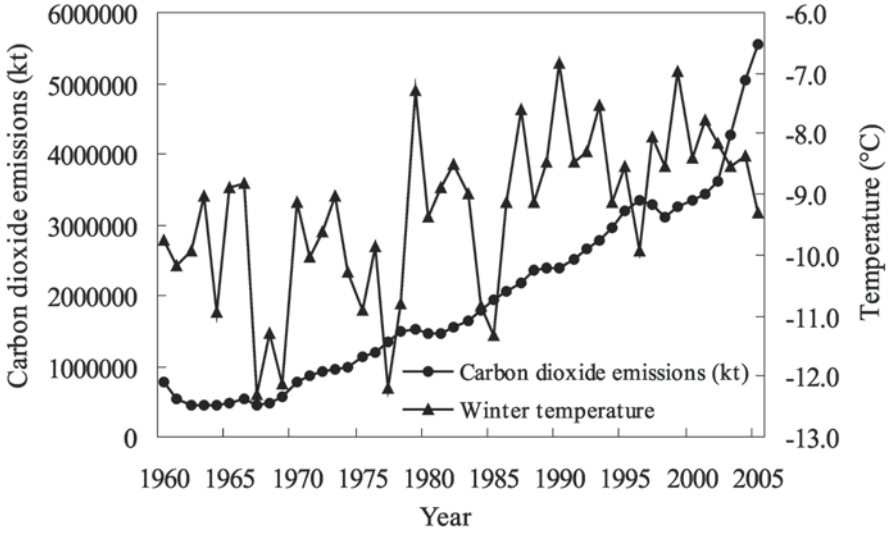

Fig. 2.20 The winter temperature in the arid region of northwest China and the yearly carbon dioxide emission in China

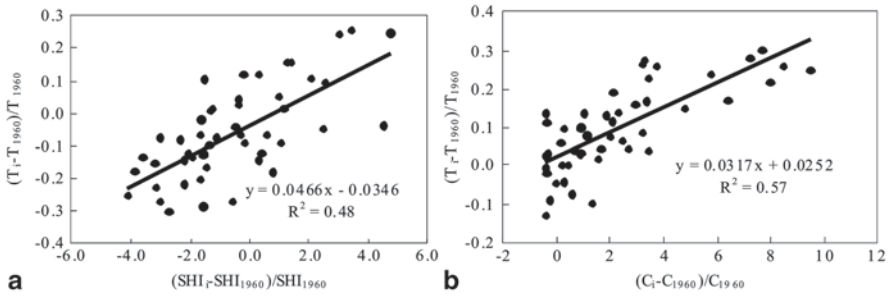

Fig. 2.21 Relationships between proportional changes of **a** annual Siberian High Index (SHI), CDE and winter temperature for the arid region of northwest China, **b** relationships between proportional changes of CDE and annual temperature for the arid region of northwest China

Siberian high index changed by 1%, the temperature of China's arid region would change by 0.0466%.

As the temperature in Northwest China dramatically changed in 1987, the 1960–1986 time frame is defined as a normal temperature fluctuation period, while 1987–2010 is defined as a climate change period. Furthermore, the contribution of the Siberian High to winter temperature change after 1987 (relative to that prior to 1987) is analyzed quantitatively.

Calculations based on a contribution rate formula and Table 2.7 indicates that the Siberian High contributed to winter temperature changes at a rate of 29.2% for the period 1987–2010.

Table 2.7 The statistical characteristics of Siberian High Index, CDE, annual temperature and winter temperature for different period

Items	1960–1986	1987–2010	Variation rate
Siberian High Index (SHI)	0.318	−0.007	102.3%
Winter temperature (°C)	−9.98	−8.35	1.63
Average annual temperature (°C)	6.25	7.20	0.94
Carbon dioxide emission (kt)	1,047,662	4,067,658	288.3%

According to the above analysis, in 1987–2010, 40.9% of the average annual temperature change was caused by winter temperature change, and 29.2% of the winter temperature change was caused by changes in the Siberian High. Hence, we can suggest preliminarily that 11.9% of the average annual temperature change was caused by changes in the Siberian High in China's northwest arid region.

2.2.4 Future Temperature Trends

2.2.4.1 Method

Wavelet Analysis As a wavelet transform can expand a time series into time frequency space, it can find localized intermittent periodicities. Wavelet analysis can also reveal localized time and frequency information without requiring the time series to be stationary. A continuous wavelet function (CWT) is described from a single function φ by translations and dilations:

$$\varphi_{a,b}(t) = |a|^{-\frac{1}{2}} \varphi\left(\frac{t-a}{a}\right), a, b \in R \tag{2.27}$$

where a is the scale parameter, b is the position parameter, and t denotes time. The CWT of the signal $f(t)$with the analyzing wavelet φ is the convolution of $f(t)$ with a set of scaled and translated wavelets:

$$W_f(a,b) = \langle f(t), \varphi_{a,b} \rangle = |a|^{-\frac{1}{2}} \int_R f(t) \varphi^* \left(\frac{t-a}{a}\right) dt \tag{2.28}$$

where * indicates the complex conjugate and $W_f(a, b)$ denotes the wavelet coefficient. Thus, the concept of frequency is replaced by that of scale, which can characterize the variation in the signal, $f(t)$, at a given time scale. The choice of wavelet φ depends on the signal to be analyzed. In this case, we select the Morlet wavelet as φ. The Morlet wavelet is defined by

$$\varphi(t) = \pi^{-1/4} e^{i\omega_0 t} e^{\left(-t^2/2\right)} \tag{2.29}$$

where ω_0 is the non-dimensional frequency (usually taken to be 6 to satisfy the admissibility). The relation between scale a and period T of the Morlet wavelet is given as: $T = \frac{4\pi a}{\omega_0 + \sqrt{2+\omega_0^2}} \approx 1.033a$ Hence, the Morlet wavelet (with $\omega_0 = 6$) and the Fourier period (T) are almost equal to the scale (a).

The wavelet variance used to detect the periods present as the power density at different time scales, a, is calculated as:

$$E_a = \frac{1}{N}\sum_{b=1}^{N}\left|W_f(a,b)\right|^2 \tag{2.30}$$

where N is the length of data. The cone of influence (COI) is the region of the wavelet spectrum in which edge effects become important. It is defined here as the e-folding time for the autocorrelation of the wavelet power at each scale. Here, COI is used to ignore the edge effects. The significance of the global wavelet spectrum is using a red noise model to compare it with the theoretical global wavelet power spectrum.

2.2.4.2 Period Analysis

The temperature change period is an important factor that affects the accuracy of temperature simulations and future projections. In our study, we performed a time-series analysis of variance extrapolation to analyze temperature change periods of river areas in the northwest arid zone. The results show that the northern slope of the Qilian Mountain, the south slope of the Altai Mountains and the northern slope of the Kunlun Mountains have the same temperature change period of 19 years, while the temperature change period in the northern slope of the Tianshan Mountains is the shortest (17 years) and that in the southern slope of the Tianshan Mountains is the longest (20 years). Overall, there is little difference among the temperature change periods for each river area.

Further, the wavelet analysis method was used to analyze temperature periodicity in the four headstreams of the Tarim River Basin (Fig. 2.22). The results show that temperature in the Aksu River Basin had two weak periods of 3 and 11 years and two strong periods of 18 and 22 years. Because the data length is only 50 years in total, 18 years was taken as a reliable period. Meanwhile, the wavelet time-frequency diagram of temperature shows that the wavelet coefficients real part of the 18-year period within the 1960–1974 and 1986–1997 time frames is in the negative phase, which indicates that, in these years, temperatures were low. Conversely, the periods of time exclusive of these years were in a positive phase, which indicates that the temperatures were high.

Temperature in the Yarkand River basin had two weak periods of 4 and 11 years and two strong periods of 17 and 22 years. In view of the data length (as mentioned

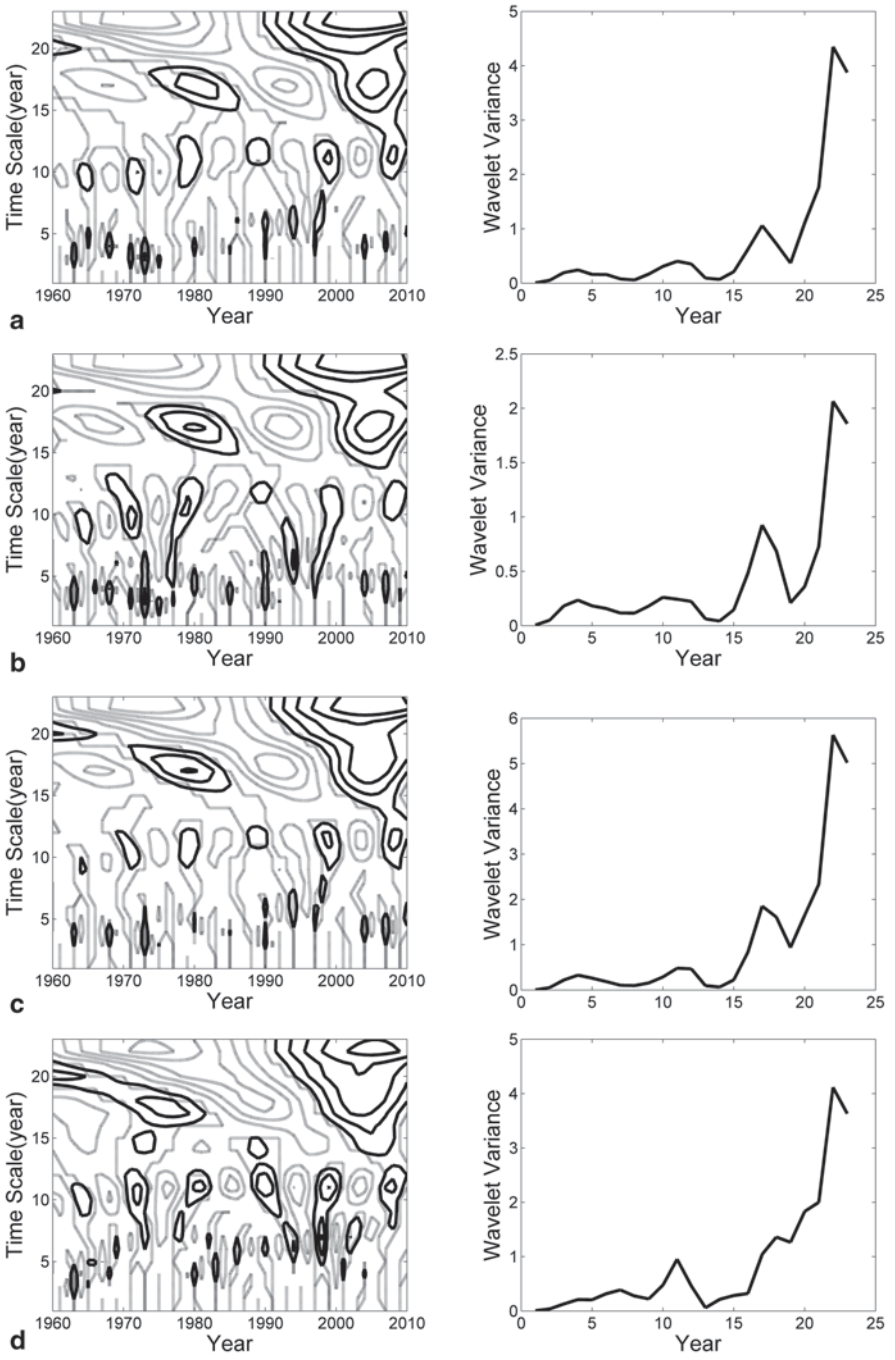

Fig. 2.22 Wavelet time-frequency distribution (*left*) and variance (*right*) of temperature in the four headstreams of Tarim river basin **a** Aksu River, **b** Yarkant River, **c** Hotan River, **d** Kaidu River

above), we considered the 17-year period as being reliable. The time-frequency distribution diagram of temperature indicated that the real part of the wavelet coefficients for the 17-year period was in a positive phase from 1973 to 1983 and again from 1997 to 2007, when temperatures were high.

Temperatures in the Hotan River basin had two weak periods of 4 and 11 years and two strong periods of 17 and 22 years, from which the 17-year period was assumed to be reliable, given the overall 50-year data collection timeframe. The real part of the wavelet coefficients of the 17-year period for the 1970–1980 and 2000–2007 stretches were in a positive phase, indicating that temperatures during these years were high.

Temperatures in the Kaidu River basin showed three weak periods of 7, 16 and 18 years and two strong periods of 11 and 18 years. In consideration of the data consistency, an 18-year cycle was taken as being reliable. The wavelet coefficient time-frequency distribution indicated that temperatures during the period 1964–1974 and after 1994 were high.

2.2.4.3 Future Temperature Forecast

To further clarify temperature changes for each river area in both historical periods and in the future, a superimposed trend prediction model was used (Table 2.2) to predict the average temperature for the next full cycle. This was then compared with the average temperatures for the period 1990–2010, the historical time period 1957–1989, and the next 10 years (2011–2020). For the 2006–2010 timeframe, simulated temperature values were used to replace temperatures where no measured data existed.

The linear regression coefficient test (Fig. 2.23) shows that the superimposed trend prediction model is highly accurate. The temperature simulation achieved $P < 0.05$ level of significance in the southern slope of the Tianshan Mountains, while other river areas reached $P < 0.01$, indicating that the model is suitable for temperature forecast in the study area.

In comparing the average temperatures in the periods 1990–2010 and 1957–1989, temperature on the southern slope of the Altai Mountains showed the greatest increase trend (Fig. 2.24), followed by temperature on the northern slope of the Qilian Mountains, the southern slope of the Tianshan Mountains, and the northern slope of the Kunlun Mountains. The temperature increments for these areas were 1.91, 0.94, 0.81 and 0.75 °C, respectively. The average temperature on the northern slope of the Tianshan Mountain increased least, with an increment of only 0.63 °C. Overall, the average temperature increased the most in northern Xinjiang, followed by the Hexi Corridor and southern Xinjiang.

A comparison of average temperatures between 2011–2020 and 1990–2010 (Fig. 2.24) shows increasing trends in the southern slope of the Altai Mountains, the northern slope of the Kunlun Mountain and the northern slope of the Tianshan Mountains, with increments of 0.76, 0.19 and 0.01 °C, respectively. However, temperatures on the southern slope of the Tianshan Mountains and the northern slope of

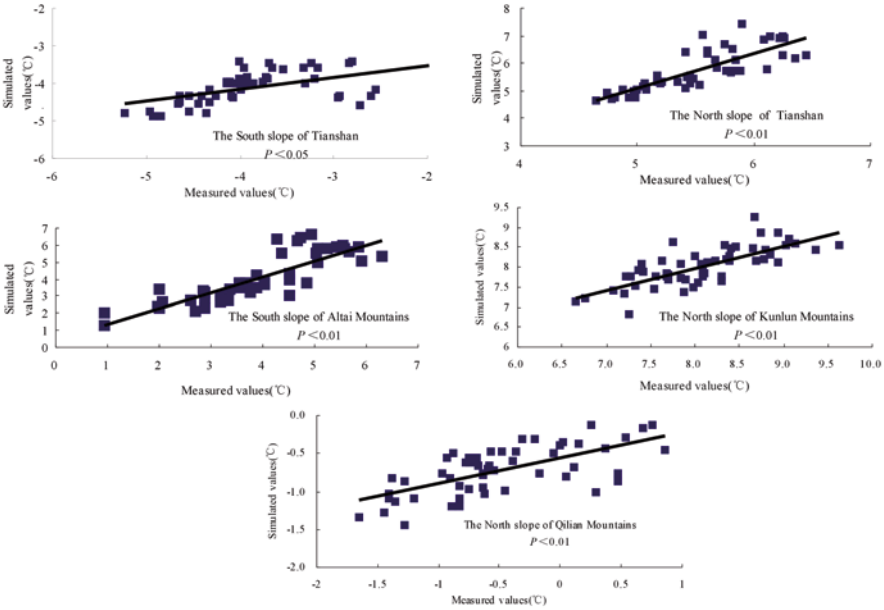

Fig. 2.23 Relations between simulated and measured values of temperature

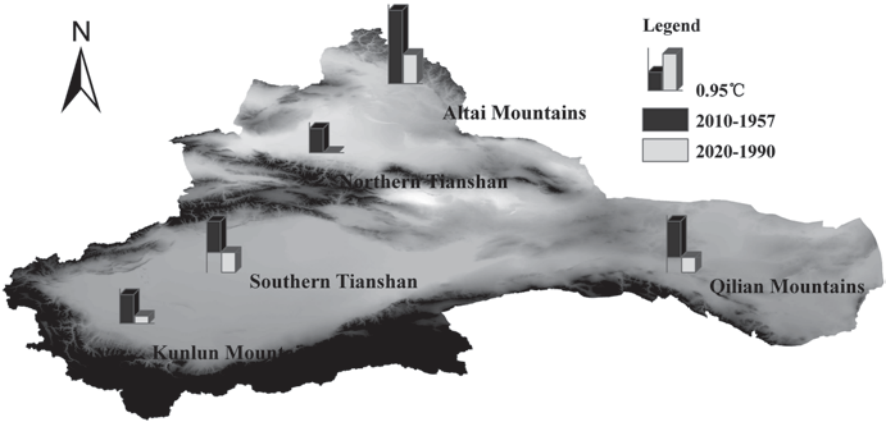

Fig. 2.24 Temperature variations in each river area in different periods

the Qilian Mountains show a decreasing trend, with decrement of 0.52 and 0.39 °C, respectively. The decreasing temperatures may be attributed to anticipated fluctuant changes in temperature during the 2011–2020 cycle's low period. Therefore, while the average temperature in some river areas may decrease over the next few years, it does not represent a long-term climate trend in the area.

2.3 Precipitation Change

Of all the natural resources required for economic development, water is the most important, particularly in arid and semi-arid regions. It is widely recognized that anthropogenic activities will affect natural ecosystem and available water resources. The most obvious activity is climate change, which has resulted in modified precipitation patterns. In recent years, the occurrence of extreme events such as droughts and floods has been on the rise worldwide. The elasticity of runoff and water resources is particularly higher for drier climates, with a higher percentage change in runoff resulting from even small changes in precipitation in arid and semi-arid regions. It is therefore very important for water resources managers to know about and prepare to deal with the effects of precipitation change on hydrological cycles and streamflow regimes (Sullivan 2001). A good place to start is to know the characteristics of precipitation changes in recent years.

In our investigation, we used the latest (1960–2010) meteorological data from meteorological stations to explore historical and predicted precipitation variations in typical river and mountain-oasis-desert areas. In addition, we analyzed relationships between and among temperature, precipitation, latitude, longitude, elevation and atmospheric circulations, and detected step changes for precipitation. The results will provide a scientific basis for predicting future climate trends and for assessing the impact of climate change on water resources.

2.3.1 Characteristics of Precipitation Change

2.3.1.1 Inter-Annual Precipitation Change

(1) Precipitation Changes in Northwest China

Over the past 50 years, mean precipitation has measured approximately 153.37 mm in China's arid northwest region. Of the 74 sites analyzed in the study area, 69 (93.24%) (Fig. 2.25) showed precipitation trending toward larger values during the 1960–2010 period, while decreases were noted at only five sites. Many of these upward trends reached the level of statistical significance ($P<0.05$, under the Mann–Kendall test); however, of the sites with trends that did not pass this level, the precipitation values increased at 30 sites (43.48%) and decreased at 4 (80%). Thus, the overall increasing rate of mean annual precipitation was 6.07 mm/10a. This trend is significant ($P<0.01$, under the Mann–Kendall test), which indicates that the climate has become wetter in the arid region.

Our study revealed varying degrees of regional differences in precipitation increases. For example, northern Xinjiang had the highest rising rate (9.20 mm/10a), followed by southern Xinjiang (5.35 mm/10a) and the Hexi Corridor of (3.96 mm/10a).

(2) Precipitation Changes in the Mountain-Oasis-Desert Area

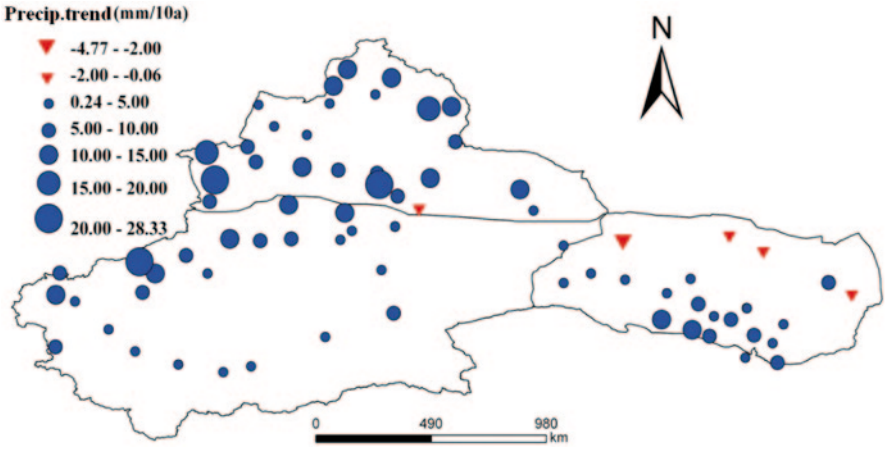

Fig. 2.25 Trends in precipitation during 1960–2010

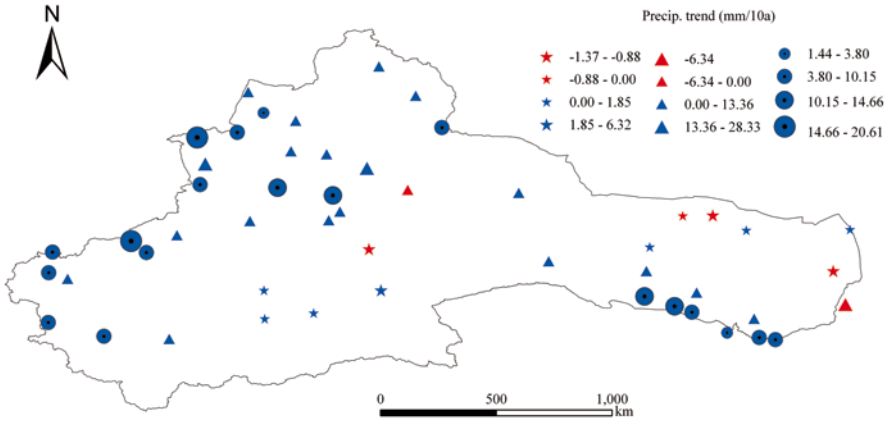

Fig. 2.26 The precipitation trend of each meteorological station during the period 1960 to 2010

Trends of Annual Precipitation The linear tendencies in precipitation measured at 51 stations over an approximate 50-year period are examined (Fig. 2.26). Among these stations, 45 had increasing trends for the period, which indicates that the overall trend is one of increased precipitation, with the mean rate at all 51 stations measuring 5.77 mm per decade.

The mountain landscape had an increasing rate of 10.15 mm per decade, the fastest among the three landscape types. This was followed by the oasis landscape at 6.29 mm per decade and the desert landscape, with only 0.87 mm per decade. The Mann–Kendall test shows that the increasing trends of the mountain and oasis landscapes are statistically significant ($P<0.01$), while the trend for the desert

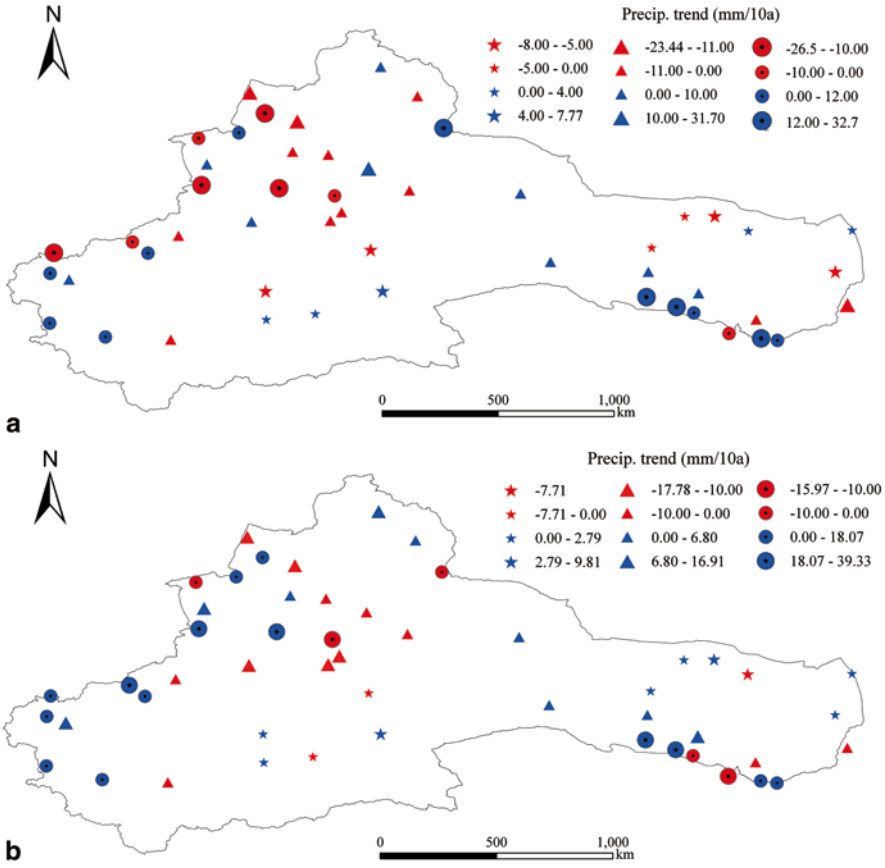

Fig. 2.27 The precipitation trend of each the meteorological station during the periods **a** 1960–1986, and **b** 1987–2010

landscape is not. There are four main reasons that explain the increasing precipitation (Yang et al. 2009): (1) local climate characteristics like high water vapor content in the air and favorable weather conditions; (2) temperature rises leading to increased amounts of glacial and snowmelt water and further promoting the formation of mountain precipitation conditions; (3) rising temperatures strengthening local circulation between the plain areas and the mountains and improving air humidity in the oasis area, leading to increased precipitation in the latter; and (4) the process of global warming-driven water circulation speeding up. Bengtsson (1997) estimated that the doubling of greenhouse gases might cause temperature rises that could increase atmospheric water vapor content by 15 % and precipitation by 8 %.

To further clarify the precipitation change of each area over different periods, the time series has been divided into two periods: 1960–1986 and 1987–2010.

During the 1960–1986 period, about a half of the 51 stations experienced increasing trends and the other half decreasing trends (Fig. 2.27a). The mean changing

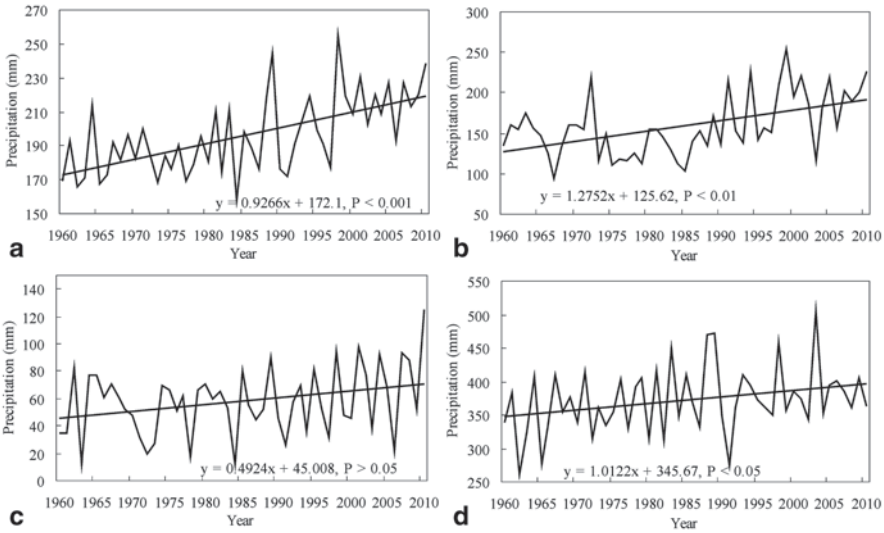

Fig. 2.28 Time series of precipitation of the snowmelt period and its linear trend for **a** entire northwest China, **b** southern Tianshan Mountains, **c** northern Kunlun Mountains, **d** northern Qilian Mountains

rate was −4.35 mm/10a. The rate of mountain landscape was 0.98 mm/10a, with 11 of 19 stations showing increasing trends. The oasis landscape had a rate of −1.17 mm/10a, with 12 of 21 stations showing decreasing trends. The desert landscape had a similar rate of −1.12 mm/10a, with 6 of 11 stations showing decreasing trends. Overall, precipitation changes across all types of landscape area were relatively insignificant during the 1960–1986 timeframe.

From 1987 to 2010, more stations (31 stations) showed increasing trends (Fig. 2.27b), with the mean rate of the 51 stations measuring 3.59 mm/10a, but precipitation changes were inconsistent across the different landscapes. The mountain areas had a rising trend with a mean rate of 12.20 mm/10a, and 14 of 19 stations had increasing trends, which was considerably more than during the 1960–1986 period. The precipitation in the oasis area jumped in 1987, and then experienced large variances while maintaining a relatively high mean (23.02 mm, considerably higher than the period of 1960–1986). Precipitation in the desert area increased slightly, at only 1.31 mm/10a. Overall, increases in precipitation during the 1987–2010 period occurred mostly in the mountain and oasis areas

Trend of Snowmelt Period Precipitation in the Mountain Area Since 1960, the mean precipitation of snowmelt shows an increasing trend in the study area, with a linear trend of 9.27 mm/10a at $P<0.001$ level in the significance test (Fig. 2.28a). The rates of increase in precipitation in southern Tianshans and the northern Qilian Mountains are higher, measuring 12.75 mm/10a and 10.12 mm/10a, respectively, and reaching a significance level of $P<0.05$. However, in the northern Kunlun

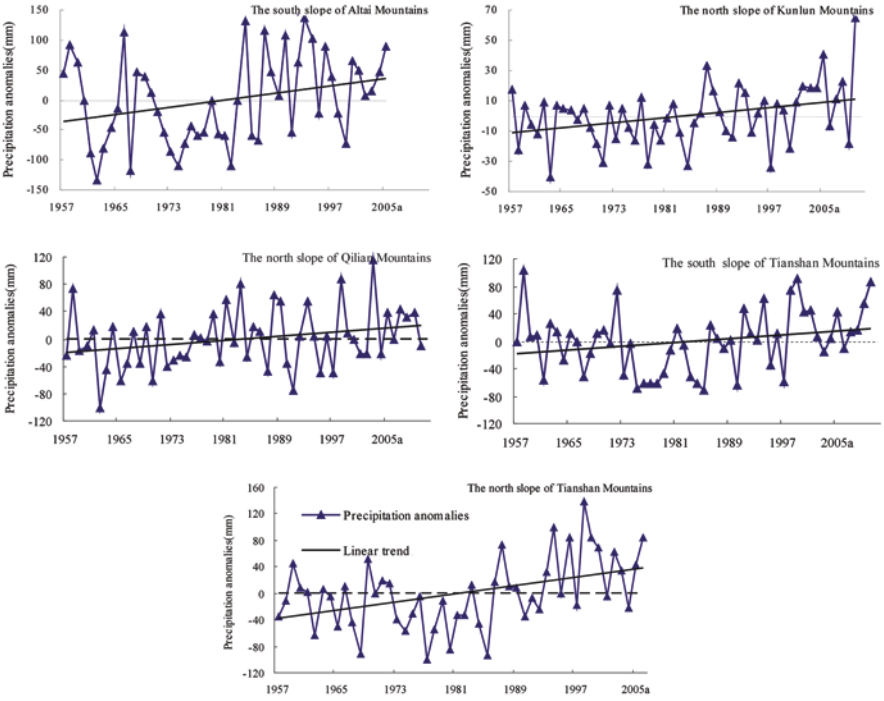

Fig. 2.29 Precipitation anomalies trends in typical river areas of the arid region of Northwest China

Mountains, the rate of increase is lower (4.92 mm/10) and does not reach significance level (Figs. 2.28b, c, d).

(3) Precipitation Changes in Typical Rivers

Precipitation Trend Precipitation in each river area shows clear increasing trends (Fig. 2.29) (Li et al. 2012). On the north slope of the Tianshan Mountain and the south slope of the Altai Mountains, the increasing trend of precipitation is statistically significant at $P<0.01$ and $P<0.05$, respectively, while trends on the north slope of the Qilian Mountains, the north slope of the Kunlun Mountains and the south slope of the Tianshan Mountains are not significant.

Since 1960, the average increasing rate of precipitation in each river area was 9.12 mm per decade. The rates of precipitation on the north slope of the Tianshan Mountains and the south slope of the Altai Mountains increased the fastest, at 15.48 and 15.30 mm/10a, respectively, followed by those on the north slope of the Qilian Mountains and the south slope of the Tianshan Mountains, at 7.64 and 6.75 mm/10a, respectively, while the north slope of the Kunlun Mountains showed increase rates of only 4.25 mm/10a.

The variation coefficient of precipitation in each river ranged from 0.12 to 0.34, which indicates moderate variability (Table 2.8). The variation coefficient on the

Table 2.8 Precipitation trends and tests in typical river areas of the arid region of Northwest China

Typical areas	Typical river areas	Cv	Zc	Step change points	Periods (a)
Hexi Corridor	The north slope of Qilian Mountains	0.12	1.25	None	22**
Northern Xinjiang	The south slope of Altai Mountains	0.26	1.97*	1987*	18**
	The north slope of Tianshan Mountains	0.17	2.64**	1992*	17*
Southern Xinjiang	The south slope of Tianshan Mountains	0.17	0.75	None	12*
	The north slope of Kunlun Mountains	0.34	1.72	1999*	20**

*$P<0.05$; **$P<0.01$

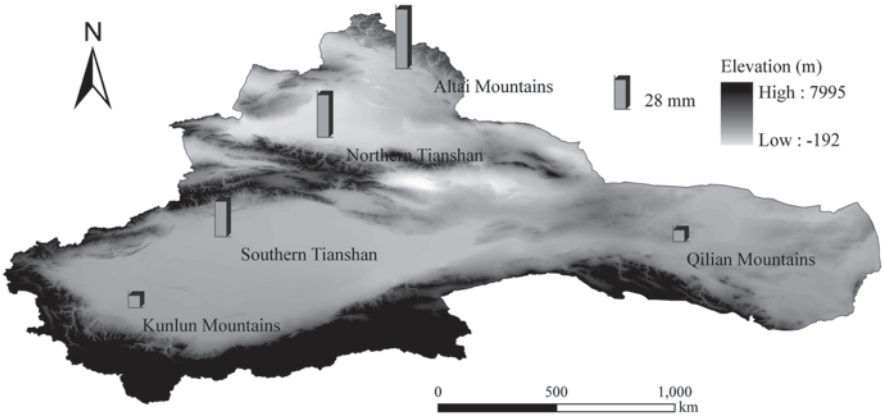

Fig. 2.30 Precipitation changes of each river in different periods in the arid region of China

northern slope of the Qilian Mountains was the smallest (0.12). while that on the northern slope of the Kunlun Mountains was the largest (0.34).

Precipitation Changes in Different Periods Compared to 1957–1989, precipitation during the period 1990–2010 on the south slope of the Altai Mountains showed the largest increase (55.41 mm) (Fig. 2.30), followed by the north and south slopes of the Tianshan Mountains, which increased by 39.56 mm and 32.91 mm, respectively. Precipitation increases on the northern slopes of the Kunlun and Qilian Mountains were the smallest, increasing by 11.33 mm and 10.77 mm, respectively. In general, northern Xinjiang registered the largest increases, followed by southern Xinjiang and the Hexi Corridor.

2.3.1.2 Seasonal Variability of Precipitation

In the 1960–2010 timeframe, spring precipitation exhibited a significant rising trend at 58 (78.38%) of the 74 sites (Fig. 2.31) while decreasing at the remaining 16 sites. Most of these upward trends are not statistically significant; however, the precipitation increases at 5 sites (8.62%) did reach significance level ($P<0.05$, under the Mann–Kendall test). Overall, the mean increasing rate in precipitation was 1.29 mm/10a for the entire northwest region. Furthermore, precipitation in northern Xinjiang showed the fastest rate of increase (2.41 mm/10a) while southern Xinjiang exhibited the slowest rate (0.55 mm/10a) (Table 2.9).

Summer precipitation increases were recorded at 54 (72.97%) of the 74 sites during the period 1960–2010 (Fig. 2.31). Precipitation values increased at 18 sites and decreased at 1, reaching significance level ($P<0.05$, under the Mann–Kendall test). The mean increasing rate in precipitation was 2.51 mm/10a in the study area, which was higher than in the other seasons. The precipitation rate increased the fastest (3.80 mm/10a) in southern Xinjiang, followed by northern Xinjiang (2.67 mm/10a) and the Hexi Corridor (0.99 mm/ 10a) (Table 2.9).

In autumn, precipitation generally trended toward larger values at 64 (86.49%) of the sites (Fig. 2.31). Although most of these trends were not at the level of statistical significance, 11 sites did achieve this level ($P<0.05$, under the Mann–Kendall test), giving an increasing rate of precipitation of 1.82 mm/10a for the entire area. Regionally, precipitation showed the fastest rate of increase (2.14 mm/10a) in northern Xinjiang, while southern Xinjiang and the Hexi Corridor were essentially the same (1.64 mm/10a).

Winter saw rising precipitation trends at 68 (91.89%) of the 74 (Fig. 2.31), with precipitation values increasing at 22 sites (32.35%), which was not at the level of statistical significance (although others did reach $P<0.05$, under the Mann–Kendall test). The mean precipitation increased 1.16 mm/10a, which was significantly lower than in spring, summer, and autumn. Regionally, northern Xinjiang showed the fastest increasing rate in precipitation (2.21 mm/10a), followed by southern Xinjiang (0.59 mm/10a) and the Hexi Corridor (0.38 mm/10a) (Table 2.9).

Correlations between elevation, longitude, latitude, AO, AAO, SO, NAO and seasonal precipitation trends were also investigated in our study (Table 2.10). We found that spring precipitation is significantly correlated with latitude ($P<0.01$), summer precipitation is strongly correlated with elevation and longitude ($P<0.05$), autumn precipitation is not significantly correlated with longitude, latitude or elevation, and winter precipitation is significantly correlated with longitude, latitude and elevation ($P<0.05$).

2.3.1.3 Decadal Variability in Precipitation

In the 1960s, the mean precipitation was 134.34 mm in China's arid northwest and showed an increasing trend through the 1970s at 60.81% of the meteorological stations. The sites showing precipitation increases were located mainly in the north

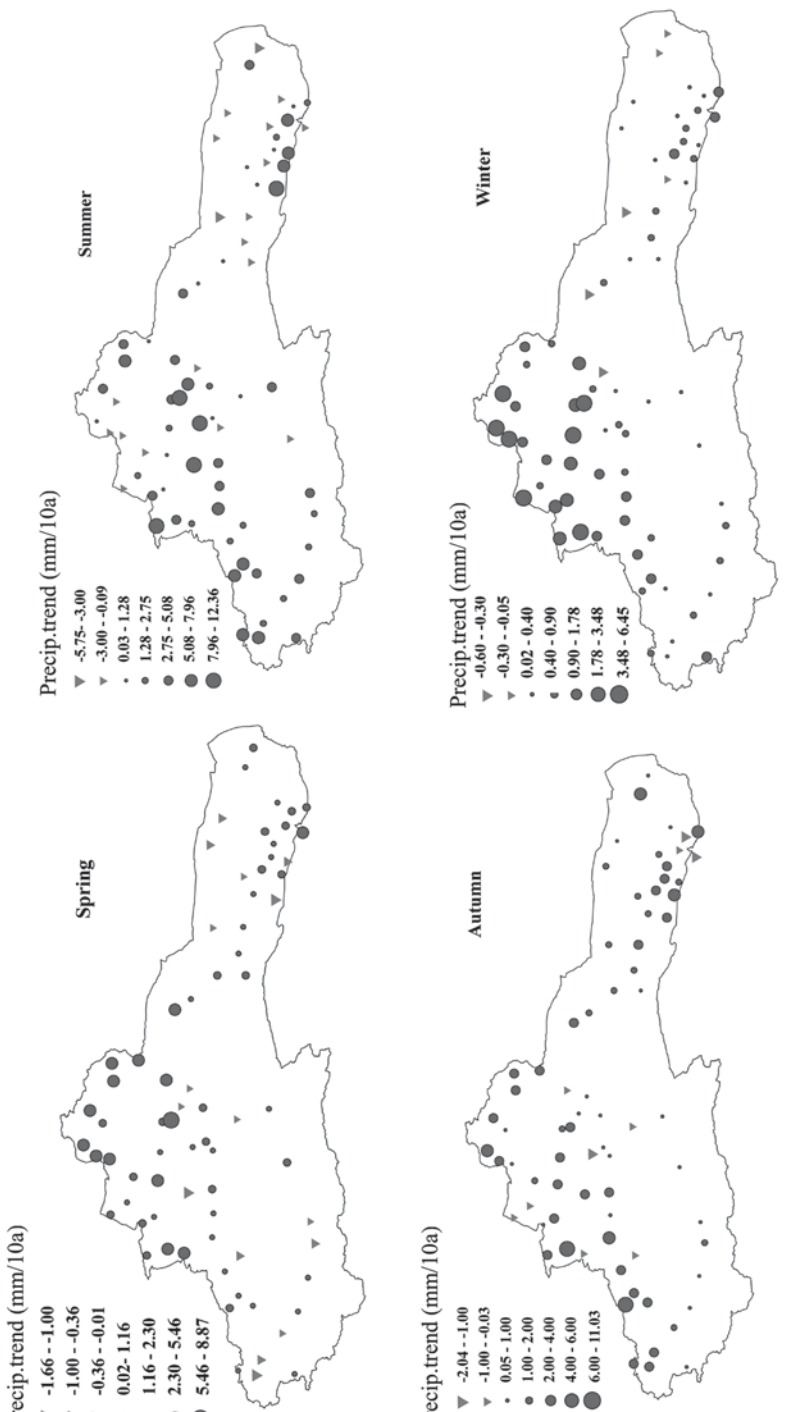

Fig. 2.31 Seasonal precipitation trends (1960–2010) in the arid region of northwest China

Table 2.9 The annual and seasonal trend in precipitation over different regions

Region	Spring (mm/10a)	Summer (mm/10a)	Autumn (mm/10a)	Winter (mm/10a)	Annual (mm/10a)
ARNC	1.29	2.51*	1.82*	1.16**	6.07**
Northern Xinjiang	2.41	2.67	2.14*	2.21*	9.20**
Southern Xinjiang	0.55	3.80*	1.64	0.59	5.35*
Hexi Corridor	0.86	0.99	1.64	0.38	3.96

*$P<0.05$; **$P<0.01$

Table 2.10 The relationship between seasonal precipitation trends and elevation, longitude, latitude and atmospheric circulation

Item	Spring	Summer	Autumn	Winter
Longitude	0.01	−0.34*	−0.13	−0.30*
Latitude	0.41**	−0.03	0.14	0.58**
Elevation	−0.18	0.35*	0.10	−0.33*
SOI	−0.18	−0.03	0.18	−0.20
AAOI	−0.02	0.04	−0.10	−0.04
NAOI	0.09	0.06	−0.17	0.14
AOI	−0.02	0.12	−0.05	0.09

*$P<0.05$; **$P<0.01$

and south slopes of the Tianshans and in the Hexi Corridor. Overall, precipitation increased the fastest in the Hexi Corridor at a rate of 8.23%, while increasing only 1.12% in southern Xinjiang and 0.36% in northern Xinjiang (Fig. 2.32).

In the 1980s, the increasing rate in precipitation was 3.91%, which is higher than the 1970s. Precipitation at 80.39% of the weather stations showed notable increases, whereas 74% of weather stations in the Hexi Corridor registered decreases. Northern Xinjiang exhibited the fastest precipitation rate increase (8.91%), followed by southern Xinxiang (8.49%). However, precipitation in the Hexi Corridor showed a decreasing trend at a rate of 3.65% (Fig. 2.32).

In the 1990s, the increasing rate of precipitation was the fastest (6.99%) compared with the other decades under study, and precipitation at 72.97% of the meteorological sites increased. Southern Xinjiang showed the fastest increasing rate (15.46%) followed by northern Xinjiang (7.63%), while the Hexi corridor trailed far behind (1.61%).

During the period 2000–2010, the mean precipitation charted a continuous increasing trend, but the increasing rate of 4.31% was less than in the 1990s. Overall, precipitation at 60.81% of the weather stations increased, while regionally, precipitation in northern Xinjiang showed the fastest increasing rate (5.08%), followed by the Hexi Corridor (4.84%) and southern Xinjiang (1.83%) (Fig. 2.32).

Fig. 2.32 Precipitation trends (1960–2010) in different decades in the arid region of northwest China

Table 2.11 Results of Mann–Kendall test for annual and seasonal precipitation and temperature

Parameter	Annual	Spring	Summer	Autumn	Winter
Precipitation (mm/decade)	8.01[b] (172.38)	1.78 (43.93)	2.55[a] (78.48)	1.72[a] (35.50)	1.73[b] (13.80)
Temperature (°C/decade)	0.35[b] (7.20)	0.24[a] (9.18)	0.26[b] (17.75)	0.41[b] (7.40)	0.39[b] (–8.83)

The data in the parenthesis are the mean of the study area
[a] delineate the significance at 5% significance level
[b] delineate the significance at 1% significance level

2.3.1.4 Spatio-Temporal Distribution of Monotonic Trends

The statistical characteristics and trends of precipitation and air temperature in the study area were examined (Table 2.11). Spatial variations are observed for precipitation trends, with few stations showing significant changes at the 0.05 significance level, although annual precipitation showed a significant positive trend (8.01 mm/decade). On a seasonal basis, statistically significant positive trends ($P<0.05$) can be detected for all seasons except for spring, with winter experiencing the most significant precipitation increases. Annually, 56% of the stations exhibited significant increasing precipitation trends at the 0.05 significance level.

Spatial trends for annual and seasonal precipitation at individual stations and on a basin scale are shown in Figs. 2.33 and 2.34. For spring, summer, autumn and winter, the percentages for all stations exhibited notable increasing trends of 6, 18, 19, and 36%, respectively (Fig. 2.33). For annual precipitation, stations in North Xinjiang and in the middle and west of the south slope of the Tianhshan Mountains showed the most significant increasing trends (Fig. 2.33a), while the basins of the Aibuhu Drainage, northern North Xinjiang (the Wulungu, Jimunai and Irtysh Rivers), and the south slope of the Tianshan Mountains (the Weigan, Aksu and Kaidu Rivers) showed strong increasing trends at a significance level of 0.01 (Fig. 2.33a).

Seasonally, the majority of the stations showed no significant trends in spring (Fig. 2.33b), with only the basins in the Chenerchen River, the Kumu Tage Desert, the Hami Basin and the Wulungu River showing statistically significant trends (at a significant level of 0.05). In summer, 18% of the stations demonstrated notable increasing trends at a 0.05 significance level, especially stations around the Tianshan Mountains and in western South Xinjiang (Fig. 2.33c). Additionally, the Kaidu River exhibited a large increase trend at the 0.01 significance level (Fig. 2.34c). In autumn, precipitation showed an increasing trend ($P<0.01$) in the Aksu River and the Bayi Basin (Fig. 2.34d), while in winter, precipitation changes were most apparent in North Xinjiang (Fig. 2.33e). Specifically, basins in North Xinjiang (except for the Ili and Wulungu Rivers), the Kaidu River and the Kumu Tage Desert exhibited the greatest statistical variations (Fig. 2.34e).

Thus, overall, we can see that precipitation in the study area was dominated by generally increasing trends, especially in North Xinjiang and the south slope of the Tianhshan Mountains. The reasons for the increase in precipitation are related to larger-scale circulation currents. The results of previous studies showed that water

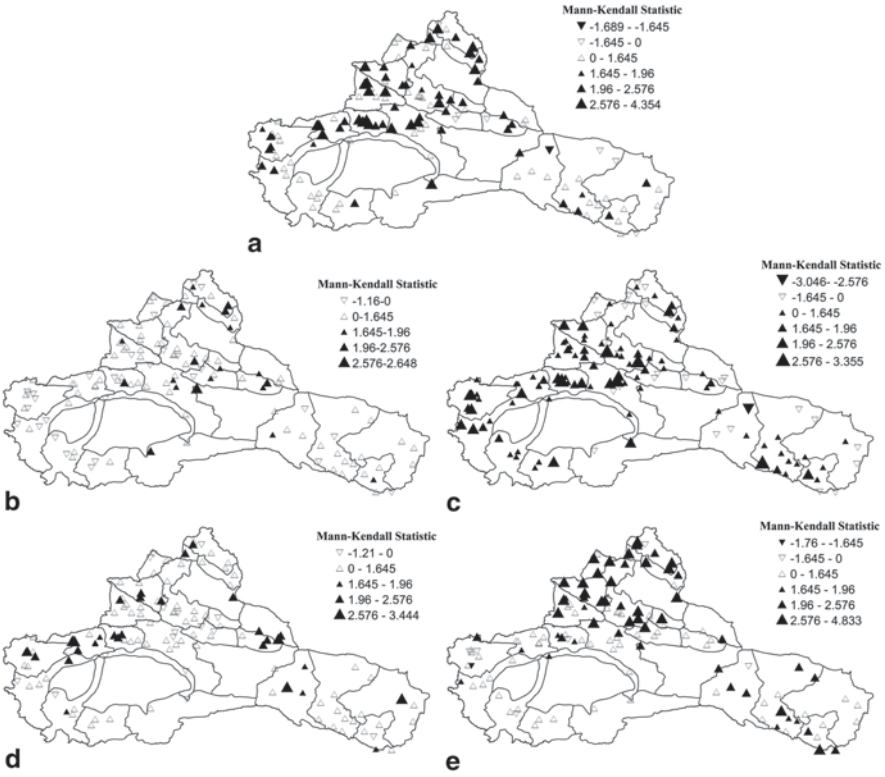

Fig. 2.33 Distribution of Mann–Kendall trends of annual and seasonal precipitation, **a** annual, **b** spring, **c** summer, **d** autumn, **e** winter

vapor from the Indian Ocean and the western Pacific has increased in recent years, bringing larger amounts of rainfall into China's arid region. However, the mixed pattern in the precipitation indicates that this change is a complex process affected both by regional atmospheric circulation and the local environment.

A detailed analysis of the relationships between trends in precipitation and elevation, and between precipitation and latitude/longitude show that precipitation is not significantly correlated with elevation (Fig. 2.35a) but is strongly correlated with latitude and longitude (Figs. 2.35b, c) ($P<0.05$).

2.3.2 Step Change Detection for Precipitation

Cumulative sum (CUSUM) charts of annual and seasonal precipitation for the study area (Fig. 2.36) showed that step changes for precipitation were identified, with the annual precipitation in 1991 at the 0.01 significance level. Annual precipitation prior to 1991 was 163 mm, whereas after 1991, it increased to 188 mm. Step changes

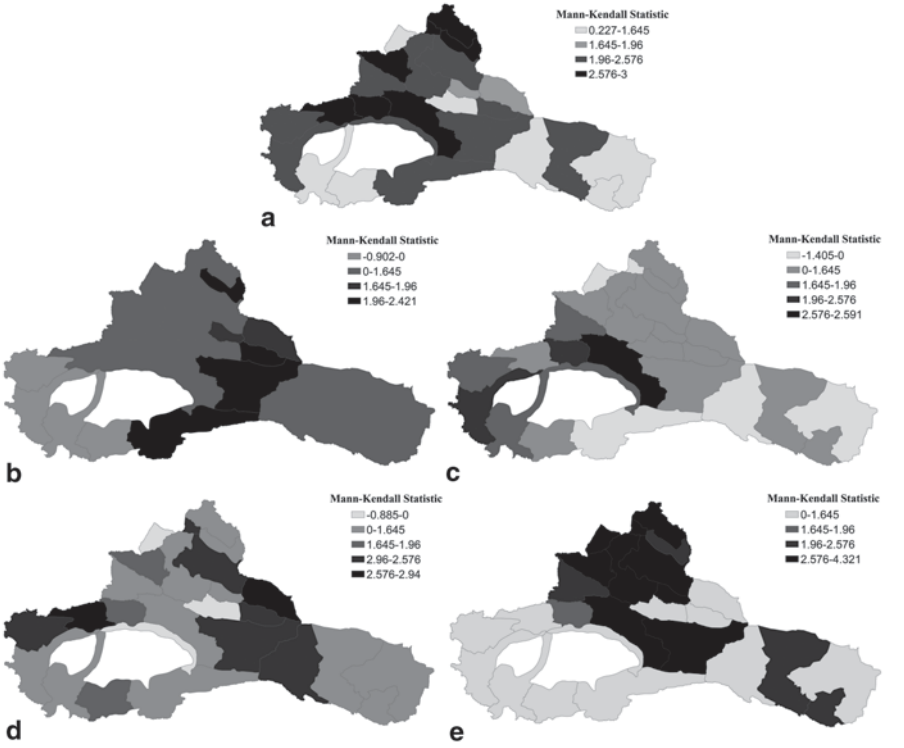

Fig. 2.34 Regional trends of precipitation at basin scale **a** annual, **b** spring, **c** summer, **d** autumn, **e** winter

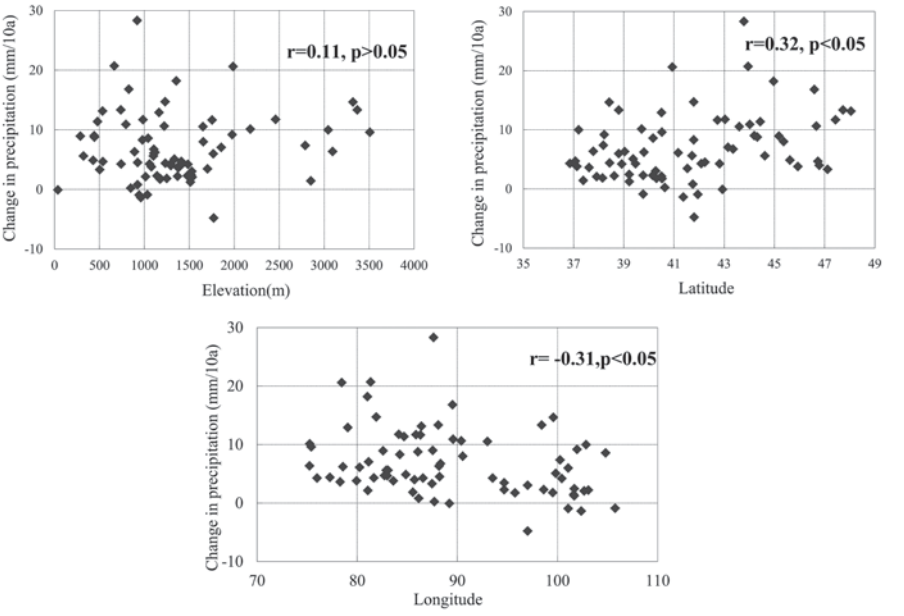

Fig. 2.35 **a** Relationships between the trends in precipitation and elevation, **b** latitude, **c** longitude

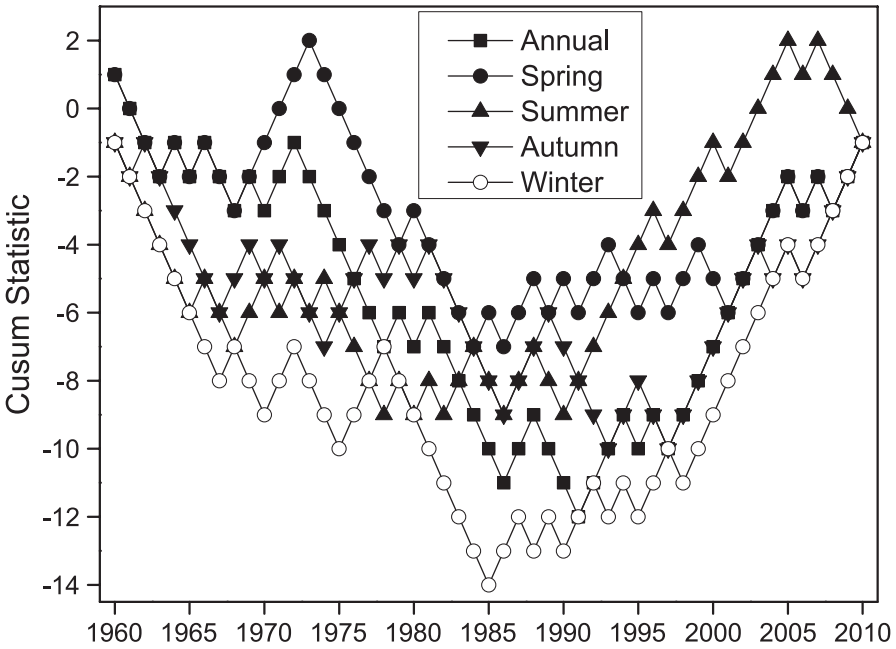

Fig. 2.36 Cumulative sum (CUSUM) charts for annual and seasonal precipitation

were also are observed in individual basins. About 12 basins showed step changes in 1986 at a significance level of 0.05, whereas only 1 basin showed changes in 1970, 1980 and 1991, respectively. On a seasonal basis, the change points can also be detected for all seasons. The change points are identified as 1986, 1990, 1997 and 1985 in spring, summer, autumn and winter, respectively; moreover, the precipitation in the later time series is higher than that in the earlier series. The step changes in individual basins on a seasonal scale show a mixed pattern, from which a uniform conclusion cannot reasonably be drawn.

The results of step change detection for precipitation (Fig. 2.37) showed that step changes were found in mountain and oasis areas in 1986 and 1987, respectively, but that no step change occurred in the desert area. For the five typical river areas, step changes in precipitation (Table 2.12) appeared in the southern slope of the Altai Mountains and the northern slope of the Tianshan Mountians in 1987 and 1992, respectively. However, no step change points were found in the northern slope of the Qilian and Kunlun Mountains or in the southern slope of the Tianshan Mountains.

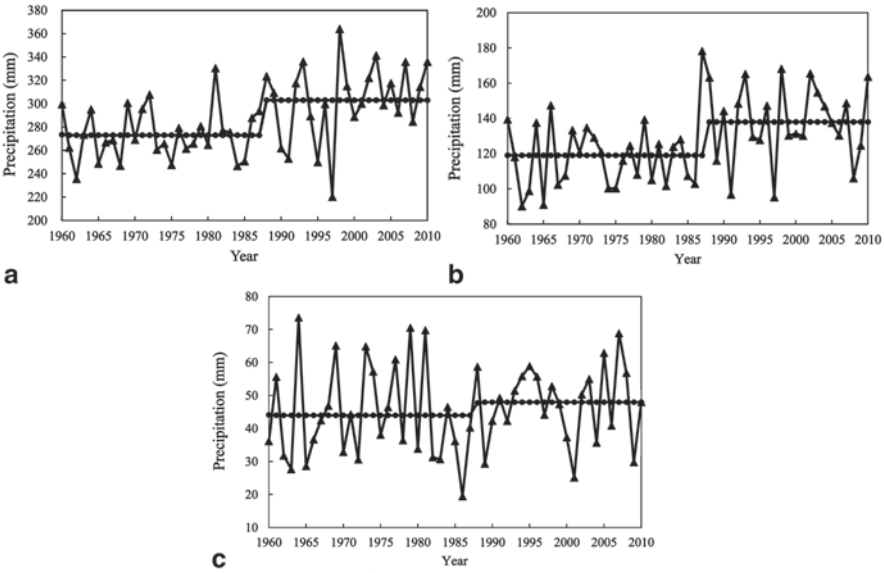

Fig. 2.37 Step change of precipitation in **a** mountains, **b** oasis, **c** desert areas

2.3.3 Future Precipitation Trends

2.3.3.1 Period Analysis

A variance analysis and an extrapolation method were employed to predict precipitation in the river areas. The results show a 22-year period as being the longest, which is predicted to occur in the northern slope of the Qilian Mountains. This will be followed by cycles of 20, 18 and 17 years in the northern slope of the Kunlun Mountains, the southern slope of the Altai Mountains and the northern slope of the Tianshan Mountains, respectively. The southern slope of the Tianshan Mountains, however, will experience a relatively short cycle of only 12 years. Overall, the precipitation periods for each river area are expected to show sizeable differences.

Further, the wavelet analysis method was used to analyze precipitation periods in the four headstreams of the Tarim River Basin (Fig. 2.38). Precipitation in the Aksu River basin had four weak periods of 4, 8, 18 and 21 years and one strong period of 11 years. Precipitation in 1962–1965, 1971–1974, 1981–1984, 1986–1991, 1997–2001 and 2001–2004 was in a positive phase, indicating that precipitation in these years was high. Precipitation in the Yarkand River basin had two weak periods of 4 and 14 years and one strong period of 9 years. Precipitation in 1962–1965, 1969–1972, 1975–1978, 1980–1983, 1984–1987, 1989–1992, 1994–1997 and 2000–2003 was in a positive phase, indicating that precipitation in these years was high. Precipitation in the Hotan River basin has four weak periods of 4, 5, 11 and 14 years and one strong period of 9 years. Precipitation in 1966–1968, 1971–1973,

Table 2.12 Precipitation trends and tests in typical river areas of the arid region of northwest China

Item	Average annual (mm)	Cv.	Trend	Zc	Step chang (year)	Primary period	Prediction model
NS of Qilian Mountians	365.69	0.120	↑	1.25	none	22**	$X(T)=392.68+1.024T+d_{t+T}$
SS of Altay Mountians	286.89	0.255	↑	1.96*	1987*	18**	$X(T)=329.456+1.03T+d_{t+T}$
NS of Tianshan Mountians	281.40	0.186	↑	2.64**	1992*	17*	$X(T)=244.449+0.822T+d_{t+T}$
SS of Tianshan Mountains	260.31	0.170	↑	0.75	none	12**	$X(T)=303.535+0.74T+d_{t+T}$
NS of Kunlun Mountains	57.03	0.340	↑	1.72	none	20**	$X(T)=62.556+0.249T+d_{t+T}$

X(T) is predicted value; T is period; d_{t+T} is the increment or decrement of period
SS southern slope, *NS* means northern slope
*$P<0.05$;**$P<0.01$

1979–1982, 1986–1988, 1989–1992, 1993–1995 and 2001–2004 was in a positive phase, indicating that precipitation in these years are high. Precipitation in the Kaidu River basin had four weak periods of 4, 9, 16 and 18 years and one strong period of 18 years. Precipitation in 1960–1970 and 1991–2002 was in a positive phase, indicating that precipitation in these years was high.

2.3.3.2 Future Precipitation Trends

The results of the linear regression coefficient test show that the period superimposed trend prediction model has a high simulation precision. Precipitation simulation reaches $P<0.05$ level of significance in the northern slope of the Tianshan Mountains, while that in the other river areas reach $P<0.01$, indicating that the model is suitable for precipitation forecast in the study area (Fig. 2.39).

In comparing average precipitation during the periods 1990–2010 and 1957–1989, we can see that precipitation increased the most in the southern slope of the Altai Mountains (Fig. 2.40) followed by the northern and southern slopes of the Tianshan Mountains, with precipitation increments of 55.41, 39.56 and 32.91 mm, respectively. Precipitation in the northern slopes of the Kunlun and Qilian Mountains increased least, with increments of only 11.33 and 10.77 mm, respectively. Overall, precipitation increased the most in northern Xinjiang, followed by southern Xinjiang and the Hexi Corridor.

In comparing average precipitation between 2011–2020 and 1990–2010, an increasing trend becomes apparent in the southern slope of the Tianshan Mountains and the northern slope of the Qilian Mountain, with respective increments of 29.29 and 18.54 mm. However, the northern slope of the Tianshan Mountains, the southern slope of the Altai Mountains and the northern slope of the Kunlun Mountains

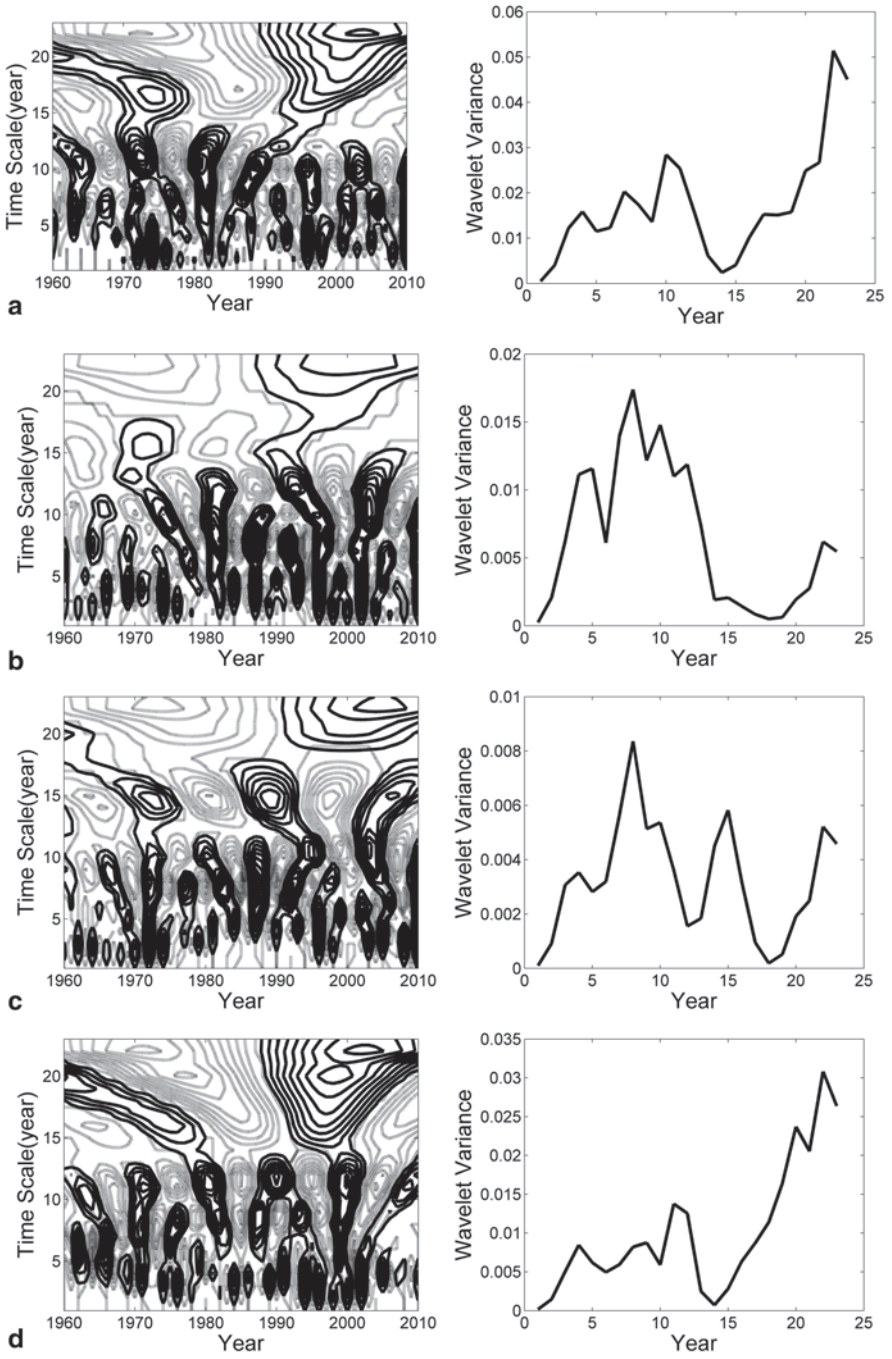

Fig. 2.38 Wavelet time-frequency distribution (*left*) and variance (*right*) of precipitation in the four headstreams of the Tarim River Basin **a** Aksu River; **b** Yarkant River; **c** Hotan River; **d** Kaidu River

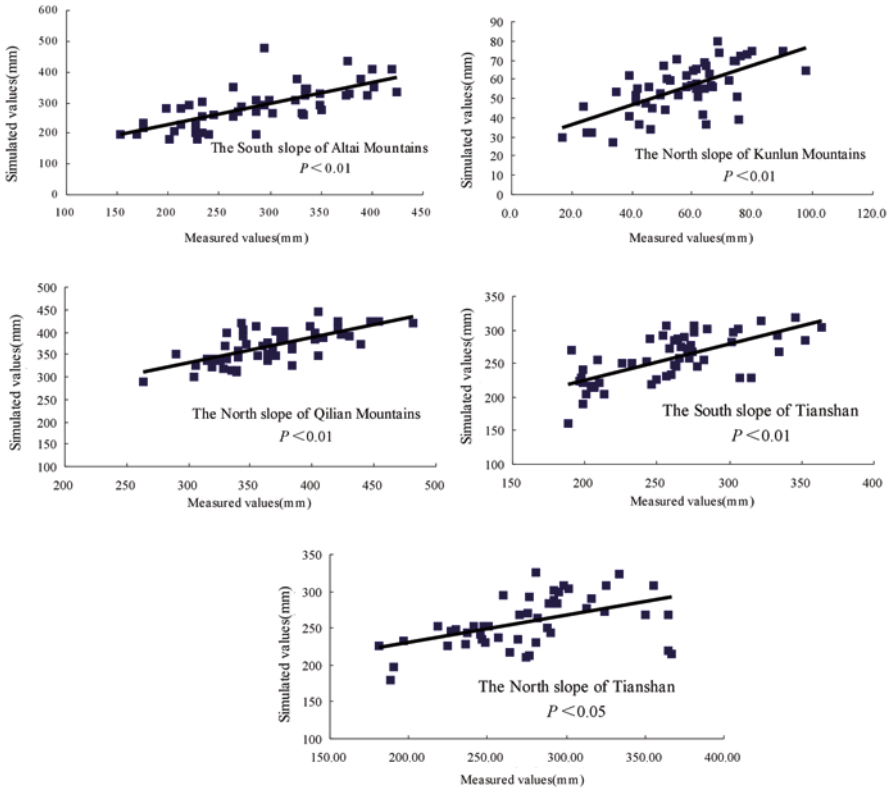

Fig. 2.39 Relations between simulated and measured values of precipitation

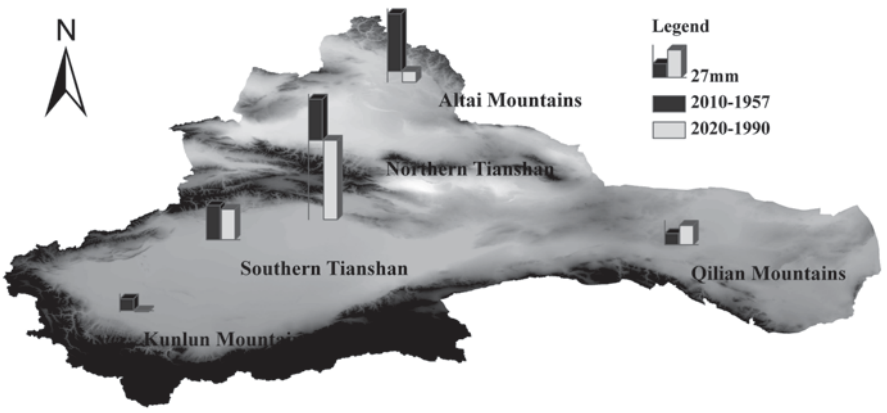

Fig. 2.40 Runoff variations of each river in different periods in the arid region

show a decreasing trend, with respective decrements of 76.32, 10.33 and 1.10 mm. The reason for decreasing precipitation may be similar to that for temperature.

2.4 Past Climate Change

Long-term climate variability is paramount for estimating the impact of climate on human activities and for predicting future climate (Rehman 2010). Because of their extensive spatial availability and high climatological sensitivity (Fritts 1976), tree rings are widely used to reconstruct past climate (Liu et al. 2006; Fang et al. 2009). Climate reconstruction using tree rings and instrumental records has revealed both fine- and coarse-scale climatic change (Moberg et al. 2005).

Previous studies in the area have mainly focused on temperature and precipitation changes and their impacts on water resources (Yuan et al. 2005; Jiang et al. 2009). However, little has yet been done in this research area with regards to the past 500 years of climate change using dendrochronology data. Detailed impact assessments require information about climatic variability at regional and national levels along with analyses not only of mean changes but also of trends (Hasanean and Basset 2006). In this research, we analyzed temporal climate variability in the study areas, placing short-term variability in a long-term context.

2.5 Temperature Variability

According to tree-ring reconstructions, the temperature in the Jing River (Fig 2.41, Yang et al. 2012) has undergone 7 warming and 7 cooling events over the past 500 years. Among the alternating warm and cold periods, three cold periods (1496–1544, 1623–1683, 1798–1850) were consistent with cold periods on the Tibetan plateau (Yang 2003) and matched glacier advancement in western China. However, only one of the cold periods (1469–1510), at Jinghe, was consistent with one of the three cold periods of the Little Ice Age in China, whereas three cold periods (1623–1683, 1798–1850, 1884–1922) were consistent with the surrounding areas in Xinjiang (Wang et al. 1998). From tree-ring reconstructions over the past five centuries, the temperature and climate change of Jinghe has not reflected the unconventional warming of recent decades. However, reconstruction of the temperatures of the past two centuries from the Qinling Mountain range TRW series showed a pronounced warming since the mid-twentieth century (Liu et al. 2009). Recent warming was shown to be unprecedented in the past 2,000 years from tree-ring chronologies in northwest Eurasia (Briffa et al. 2008) and western China (Holmes et al. 2009).

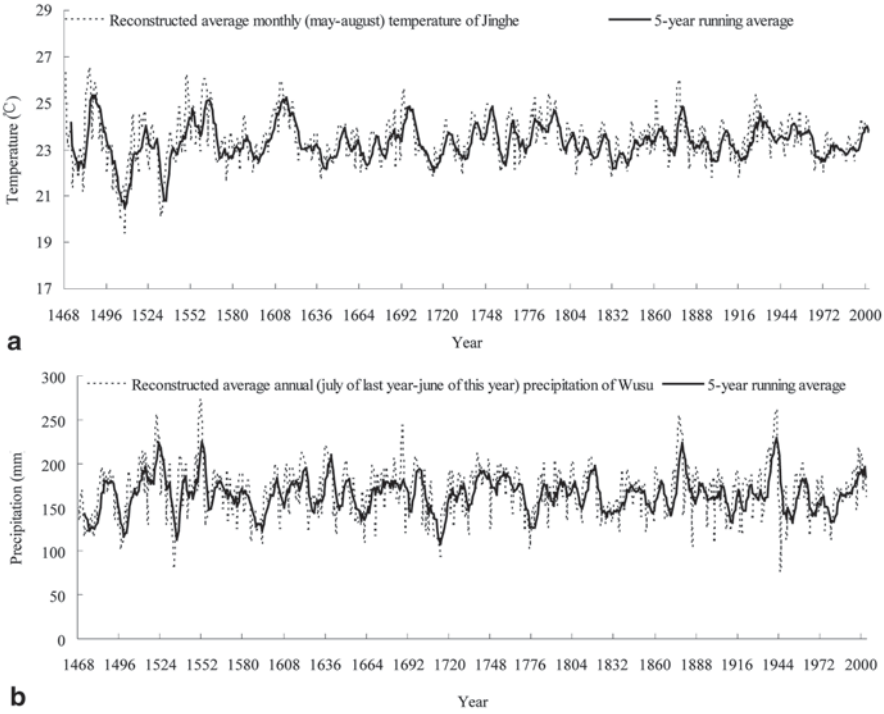

Fig. 2.41 Reconstructed **a** AMT of Jinghe, **b** ANP at Wusu in northern Xinjiang

2.6 Precipitation Variability

Tree-ring reconstructions of the precipitation at Wusu from the past 500 years (Fig. 2.41, Yang et al. 2012) have shown 9 wet periods and 9 drought events. Among the alternating wet and dry periods, wet periods were dominant prior to 1820, followed by mainly dry periods. In contrast, the occurrences of wet and dry periods in Shanxi (Li et al. 2006) were negatively correlated to those of Jinghe in northern Xinjiang.

2.7 Extreme Temperature and Precipitation

The maximum temperatures of recent years are lower than those of the past 500 years, while recent minimum temperatures are higher. Similarly, the maximum precipitation of recent years is lower than that of the past 500 years, while minimum precipitation is higher (Table 2.13, Yang et al. 2012).

Table 2.13 Extreme temperature (T) and precipitation (P)

Item	Max T (May–August) °C	Min T °C	Max P (July of previous year to June of current year) (mm)	Min P (July of previous year to June of current year) (mm)
Past 500–year history	26.6	19.4	273	219
Recent 40 years	24.5	22.0	76	113

These findings suggest that northern Xinjiang is located within a unique geographic unit that is collectively representative of China and global patterns, but conforms to patterns established in the surrounding areas of Xinjiang and the Tibetan plateau. Furthermore, data for Jinhe and Wusu do not show abnormal contemporary warming and wetting trends, and recent temperature and precipitation variability does not exceed variability ranges in the 500-year period under investigation.

Summary

1. Over the past 50 years, the temperature in the arid region of Northwest China has shown a significant increasing trend ($P<0.01$), at a rate of 0.343 °C/10a. Regionally, temperature increases reveal strong regional differences. The temperature in northern Xinjiang increased the fastest, at a rate of 0.386 °C/10a, followed by increased temperature rates in the Hexi Corridor (0.352 °C/10a) and in southern Xinjiang (0.283 °C/10a). Among the three landscape types (mountains-oasis-desert), the desert has the highest rate of increase (0.360 °C per decade), followed by the oasis region (0.339 °C per decade) and the mountain area (0.325 °C per decade). In addition, analyses of seasonal variability exhibited an increasing rate of mean air temperature of 0.486 °C/10a, which is higher than that in spring, summer, or autumn. The increasing rate of temperature in northern Xinjiang is the highest (0.587 °C/10a) in winter, followed by the rate in the Hexi Corridor (0.486 °C/10a), while Southern Xinjiang has the lowest rate (0.385 °C/10a). The winter temperature of the arid region of northwest China has a strong and significant correlation with the Siberian High Index and China's carbon dioxide emissions.
2. The Mann–Kendall method was used to detect step changes in temperature. Results show that a step change probably occurred in 1988 ($P<0.01$) for regional annual air temperature, while step changes in 1998, 1996, 1987 and 1986 ($P<0.05$) were detected in spring, summer, autumn and winter for the whole region, respectively. In selecting time-series analysis of variance extrapolation to analyze temperature change periods, we found that each river basin exhibited changes around every 17 to 20 years.
3. Mean precipitation has been calculated at about 153.37 mm for the past 50 years, with the increasing rate of mean annual precipitation measuring 6.07 mm/10a and a precipitation step change occurring in 1991. There are some regional differences in precipitation increases. For instance, the northern Xinjiang has the highest rate of increase (9.20 mm/10a), followed by southern Xinjiang (5.35 mm/10a) and the Hexi Corridor (3.96 mm/10a). In addition, from our

analysis of seasonal variability, we found that summer-time precipitation had the largest rate (2.51 mm/10a), followed by autumn and spring, and that winter had the smallest rate (1.16 mm/10a).

4. The variance analysis for precipitation indicated that the 22-period in the northern slope of the Qilian Mountains was the longest, followed by the northern slope of the Kunlun Mountains, the southern slope of the Altai Mountains and the northern slope of the Tianshan Mountains, with cycles of 20, 18 and 17 years, respectively.
5. Climate reconstruction using tree rings and instrumental records have revealed both fine- and coarse-scale climatic change. According to tree-ring reconstructions, the temperature in the Jing River has undergone 7 warming and 7 cooling events over the past 500 years, while tree-ring reconstructions of precipitation at Wusu have shown 9 wet periods and 9 drought events.

References

Abouabdillah A, Oueslati O, De Girolamo AM, Lo Porto A (2010) Modeling the impact of climate change in a mediterranean catchment (Merguellil, Tunisia). Fresenius Environ Bull 19:2334–2347

Ashrafi K, Shafiepour M, Ghasemi L et al (2012) prediction of climate change induced temperature rise in regional scale using neural network. Int J Environ Res 6(3):677–688

Bengtsson L (1997) The numerical simulation of climatic change. Ambio 26:58–65

Beniston M, Rebetez M (1996) Regional behavior of minimum temperature in Switzerland for the period 1979–1993. Theor Appl Climatol 53:231–243

Briffa KR, Melvin TM, Vaganov EA, Grudd H et al (2008) Trends in recent temperature and radial tree growth spanning 2,000 years across northwest Eurasia. Philos Trans R Soc B 363:2271–2284

Brohan P, Kennedy JJ, Harris I, Tett SFB, Jones PD (2006) Uncertainty estimates in regional and global observed temperature changes: a new data set from 1850. J. Geophys Res-Atmos 111:D12106. doi:10.1029/2005JD006548

Chen ZQ, He YS, Yan JP (1984) Arid climate and the regulation of the hydrothermal resources in the Northwest China. J Desert Res 14(4):108–112

Crowley TJ (2000) Causes of climate change over the past 1000 years. Science 289(5477):270–277

D'Arrigo R, Jacoby G, Wilson R, Panagiotopoulos F (2005) A reconstructed Siberian High index since A.D.1599 from Eurasian and North American tree rings. Geophys Res Lett 32:L05705. doi:10.1029/2004GL022271

Fang KY et al (2009) Drought variations in the eastern part of northwest China over the past two centuries: evidence from tree rings. Clim Res 38:129–135

Fritts HC (1976) Tree rings and climate. Academic Press, New York

Gong DY, Ho CH (2002) The Siberian High and climate change over middle to high latitude Asia. Theor Appl Climatol 72(1–2):1–9

Guo J (2010) Research on the effects of climate change on water cycle and water resources. Wuhan University, Ph. D. Thesis

Hasanean HM, Basset HA (2006) Variability of summer temperature over Egypt. Int J Climatol 26:1619–1634

He YQ, Lu AG, Zhang ZL, Pang HX, Gu J (2005) Seasonal variation of regional warming-up structure across China in the past half century. Clim Res 28:213–219

Holmes JA, Cook ER, Yang B (2009) Climate change over the past 2,000 years in western China. Quat Int 194:91–107

Intergovernmental Panel on Climate Change (IPCC) (2007) Climate change 2007: the physical science basis. In: Solomon S et al (ed) Contribution of working group I to the Fourth Assessment Report of the intergovernmental panel on climate change. Cambridge University Press, Cambridge, pp 996

Jiang FQ, Li XM, Wei BG, Hu RJ (2009) Observed trends of heating and cooling degree-days in Xinjiang Province, China. Theor Appl Climatol 97:349–360

Li Q, Liu Y, Cai QF, Sun JV et al (2006) Reconstruction of annual precipitation since 1686 A. D. from Ningwu region, ShanxiI province. Quat Sci 26(6):999–1006

Li QH, Chen YN, Shen YJ et al (2011) Spatial and temporal trends of climate change in Xinjiang, China[J]. J Geogr Sci 21(6):1007–1018

Li BF, Chen YN, Shi X, Chen ZS, Li WH (2012a) Temperature and precipitation changes in different environments in the arid region of northwest China. Theor Appl Climatol, doi:10.1007/s00704-012-0753–4

Li BF, Chen YN, Shi X (2012b) Why does the temperature rise faster in the arid region of northwest China? J Geophys Res 117:D16115. doi:10.1029/2012 JD017953

Li Dongliang, Peng Suqin, Yao Hui (1995) The climate characteristics of winter mean temperature in northwestern China. Atmospheric Sci 19(22):192–199

Li D, Wei L, Cai Y et al (2003) The present facts and the future tendency of the climate change in Northwest China. J Glaciol Geocryol 25(2):135–142

Liu X, Yin ZY, Shao X, Qin N (2006) Temporal trends and variability of daily maximum and minimum, extreme temperature events, and growing season length over the eastern and central Tibetan Plateau during 1961–2003. J Geophys Res 111:D19109

Liu Y, Linderholm HW, Song H, Cai Q et al (2009) Temperature variations recorded in Pinus tabulaeformis tree rings from the southern and northern slopes of the central Qinling Mountains, central China. Boreas 38:285–291

Lu AG (2009) Impacts of global warming change on patterns of temperature in China. J Mt Sci 6:405–410

Mahlstein I, Knutti R (2010) Regional climate change patterns identified by cluster analysis. Clim Dynam 35(4):587–600

Mariotti L, Coppola E, Sylla M B, et al.(2011) Regional climate model simulation of projected 21st century climate change over an all-Africa domain: Comparison analysis of nested and driving model results[J]. J Geophys Res Atmos 116 (D15, 16)

Moberg A, Sonechkin DM, Holmgren K, Datsenko NM et al (2005) Highly variable northern hemisphere temperatures reconstructed from low- and high-resolution proxy data. Nature 433:613–617

Moriondo M, Bindi M, Fagarazzi C et al (2011) Framework for high-resolution climate change impact assessment on grapevines at a regional scale. Reg Environ Chang 11(3):553–567

Panagiotopoulos F, Shahgedanova M, Hannachi A, Stephenson DB (2005) Observed trends and teleconnections of the Siberian high: a recently declining center of action. J Clim 18(9):1411–1422

Pierce DW, Barnett TP, Santer BD et al (2009) Selecting global climate models for regional climate change studies[J]. Proc Natl Acad Sci USA 106(21):8441–8446

Rehman S (2009) Study of Saudi Arabian climatic conditions using Hurst exponent and climatic predictability index. Chaos Soliton Fract 39(2):499–509

Rehman SFQ (2010) Temperature and rainfall variation over Dhahran, Saudi Arabia, (1970–2006). Int J Climatol 30:445–449

Rehman S, Siddiqi AH (2009) Wavelet based hurst exponent and fractal dimensional analysis of Saudi climatic dynamics. Chaos Soliton Fract 40(3):1081–1090

Ren GY, Xu MZ, Chu ZY, Guo J, Li QX, Liu XN, Wang Y (2005) Changes of surface air temperature in China during 1951–2004 (In Chinese with English abstract). Clim Envir Res 10(4):717–727

Ruelland D, Ardoinbardin S, Billen G et al (2008) Sensitivity of a lumped and semi-distributed hydrological model to several methods of rainfall interpolation on a large basin in West Africa. J Hydrol 361(1/2):96–117

Shi YF, Shen YP, Hu RJ (2002) Preliminary study on signal, impact and foreground of climatic shift from warm-dry to warm-humid in Northwest China. J Glaciol Geocryol 24(3):219–226

Shi YF, Shen YP, Li DL (2003) Discussion on the present climate change from warm-dry to warm-wet in northwest China. Quat Sci 23(2):152–164

Shi YF, Shen YP, Kang E, Li DL, Ding YJ, Zhang GW, Hu RJ (2007) Recent and future climate change in northwest china. Clim Chang 80(3–4):379–393

Shi YF, Zhang XS (1995) Impact of climate-change on surface-water resource and tendency, in the future in the arid zone of Northwestern China. Sci China 38(11):1395–1408

Segev U (2010) Regional patterns of ant-species richness in an arid region: the importance of climate and biogeography. J Arid Environ 74(6):646–652

Stahlschmidt ZR, DeNardo DF, Holland JN, Kotler BP, Kruse-peeples M (2011) Tolerance mechanisms in North American deserts: Biological and societal approaches to climate change. J Arid Environ 75(8):681–687

Sullivan C (2001) The potential for calculating a meaningful water poverty index. Water Int 26(4):471–480

Sun F, Roderick ML, Farquhar GD, Lim WH, Zhang Y, Bennett N, Roxburgh SH (2010) Partitioning the variance between space and time. Geophys Res Lett 37:L12704. doi:10.1029/2010GL043323

Tebaldi C, Smith RL, Nychka D et al (2005) Quantifying uncertainty in projections of regional climate change: A Bayesian approach to the analysis of multimodel ensembles[J]. J Clim 18(10):1524–1540

Vuille M, Bradley RS (2003) 20th century climate change in the tropical Andes: observations and model results. Clim Chang 59:75–99

Wang SU, Ye JL, Gong DY (1998) Climate in China during the Little Ice Age. Quat Sci 1:54–64

Wang JS, Fei XL, Wei F (2008) Further study of temperature change in northwest China in recent 50 years. J Desert Res 28(4):724–732

Xu Y, Ding YH, Zhao ZC (2003) Scenario of temperature and precipitation changes in Northwest China due to human activity in the 21~ (st) Century. J Glaciol Geocryol 23(5):327–330

Yang B (2003) Climate history of the Tibetan plateau during the last two millennia. Adv Earth Sci 18(2):285–291

Yang Y, Chen Y, Li W, Yu S, Wang M (2012) Climatic change of inland river basin in arid area: a case study in northern Xinjiang, China. Theor Appl Clim 107:143–154

Yuan YJ, Xie GH, Wei WS, Zhang JB (2005) Similarities and differences between summer temperature changes in Tianshan mountainous region and southern and northern Xinjiang. Meteorol Sci Technol 33(2):152–155

Zhang LY, Jiang ZL (1992) The genesis of the arid climate of northwestern China. Arid Land Geogr 15(2):1–12

Zhang XG, Li XQ (1982) Some characteristics of temperature variation in China in the present century. Acta Meteorol Sin 20(2):198–208

Zhang Q, Hu YQ, Cao XY et al (2000) On some problems of arid climate system of Northwest China. J Desert Res 20(4):357–362

Zhang Q, CJ Zhang CJ, Bai HX, Lin L, Sun LD, Liu DX, Wang JS, Zhao HY (2010a) New development of climate change in Northwest China and its impact on arid environment. J Arid Meteorol 28(1):1–7

Zhang XQ, Sun Y, Mao WF, Liu YY, Ren Y (2010b) Regional response of temperature change in the arid regions of China to global warming. Arid Zone Res 27(4):592–599